ANKARA YILDIRIM BEYAZIT UNIVERSITY
GRADUATE SCHOOL OF NATURAL AND APPLIED SCIENCES

LOW-COMPLEXITY APPROACHES FOR FASTER-THAN-NYQUIST SIGNALING

Ph.D. Thesis by

Adem ÇİÇEK

Department of Electrical Electronics Engineering

August, 2023

ANKARA

LOW-COMPLEXITY APPROACHES FOR FASTER-THAN-NYQUIST SIGNALING

A Thesis Submitted to the

Graduate School of Natural And Applied Sciences of

Ankara Yildirim Beyazit University

In Partial Fulfillment of the Requirements for the Degree of Doctor of Philosophy in Electrical Electronics Engineering, Department of Electrical Electronics Engineering

by

Adem ÇİÇEK

August, 2023

ANKARA

Ph.D. THESIS EXAMINATION RESULT FORM

We have read the thesis entitled "**LOW-COMPLEXITY APPROACHES FOR FASTER-THAN-NYQUIST SIGNALING**" completed by **ADEM ÇİÇEK** under supervision of **PROF. DR. ENVER ÇAVUŞ** and we certify that in our opinion it is fully adequate, in scope and in quality, as a thesis for the degree of Doctor of Philosophy.

Prof. Dr. Enver ÇAVUŞ

Supervisor

Prof. Dr. Asaf Behzat Şahin

Thesis Committee Member

Assoc. Prof. Dr. Serdar Özyurt

Thesis Committee Member

Prof. Dr. Bülent TAVLI

Examining Committee Member

Assoc. Prof. Dr. Yaser DALVEREN

Examining Committee Member

Prof. Dr. Sadettin ORHAN

Director

Graduate School of Natural and Applied Sciences

ETHICAL DECLARATION

I hereby declare that, in this thesis which has been prepared in accordance with the Thesis Writing Manual of Graduate School of Natural and Applied Sciences,

- All data, information and documents are obtained in the framework of academic and ethical rules,
- All information, documents and assessments are presented in accordance with scientific ethics and morals,
- All the materials that have been utilized are fully cited and referenced,
- No change has been made on the utilized materials,
- All the works presented are original,

and in any contrary case of above statements, I accept to renounce all my legal rights.

Date: 2023, 28 August **Signature:** _____

Name & Surname: Adem ÇİÇEK

ACKNOWLEDGEMENTS

I would like to express my heartfelt gratitude to my advisor, Prof. Dr. Enver ÇAVUŞ, whose unwavering support guided me throughout my Ph.D. journey.

I would like to convey my appreciation to the esteemed members of our committee, Assoc. Prof. Dr. Serdar ÖZYURT, Prof. Dr. Asaf Behzat ŞAHİN, Prof. Dr. Bülent TAVLI, and Assoc. Prof. Dr. Yaser DALVEREN, for their valuable insights and feedback. I also want to express my gratitude to Asst. Prof. Dr. Mehmet ÖZBEK, who previously served as a thesis committee member, for his significant contributions.

In addition to my advisor and committee members, I am deeply thankful to my coauthors, Prof. Dr. Halim YANIKOMEROGLU and Assoc. Prof. Dr. Ian D. MARSLAND at Carleton University and Asst. Prof. Dr. Ebrahim BEDEER at the University of Saskatchewan, for their invaluable assistance and guidance in exploring the realm of faster-than-Nyquist signaling.

I want to express my appreciation to my other coauthors, Abdulsamet ÇAĞLAN and Emre ÇERÇİ, from Ankara Yildirim Beyazit University, for their camaraderie and support.

Furthermore, I am thankful to Cankiri Karatekin University, my current workplace, and Ankara Yildirim Beyazit University for their support and research facilities.

I would also like to express my gratitude for the support provided by the Scientific and Technological Research Council of Turkiye (TUBITAK) with the grant number 1059B141900454.

Last but not at least, I am deeply indebted to my parents for their unwavering well wishes and support throughout my life. I also extend my appreciation to my parents-in-law, my wife, and my kids for their understanding and encouragement.

August, 2023 **Adem ÇİÇEK**

LOW-COMPLEXITY APPROACHES FOR FASTER-THAN-NYQUIST SIGNALING

ABSTRACT

A promising avenue to achieve higher data rates is through the adoption of a non-orthogonal physical layer transmission approach known as Faster-than-Nyquist (FTN) signaling, which holds the potential to transmit more data with identical bit energy and bandwidth utilization compared to Nyquist signaling. However, FTN signaling introduces complexity to the system due to interference. This thesis initiates an exploration into the impact of channel coding, including non-binary and binary low-density parity-check codes, as well as polar codes, on a low-complexity FTN detector. The simulation results reveal that channel coding effectively narrows the performance gap between the FTN detector and the optimal BCJR detector. Consequently, there is no imperative need for a high-complexity FTN detector, particularly when dealing with high values of τ, referred to as the acceleration or packaging parameter. Additionally, the thesis introduces a coordinate interleaved FTN signaling technique, upon which a low-complexity FTN detector is formulated and compared with existing literature. This innovative approach yields a 10% increase in spectral efficiency (SE) at a relatively modest cost of 0.6 dB. In essence, this detector strikes a favorable balance between performance and complexity. Furthermore, the thesis addresses FTN signaling detection as a semidefinite problem and proposes a low-complexity soft-output semidefinite relaxation (SDR) based detector for M-PAM, supported by lookup tables (LUTs). Simulation results demonstrate that this detector, with polynomial computational complexity and adaptability to higher modulation schemes, closely approximates the coded BCJR performance within 0.8 dB for 4-PAM. Moreover, it achieves a 0.3 dB improvement in performance when SNR-based LUTs are employed. Given its low complexity nature, this suggests that the soft-output SDR detector can provide good performance for high modulation in terms of the produced log-likelihood ratios (LLRs).

Keywords: Faster-than-Nyquist signaling, channel coding, semidefinite relaxation, non-orthogonal physical layer transmission technique, convex optimization.

NYQUIST'DEN DAHA HIZLI SİNYALLEŞME İÇİN DÜŞÜK KARMAŞIKLI YAKLAŞIMLAR

ÖZ

Daha yüksek veri hızlarına ulaşmanın umut verici bir yolu, Nyquist sinyalleşmesine göre daha fazla veriyi aynı bit enerjisi ve bant genişliği kullanımı ile iletebilme potansiyeline sahip Nyquist'ten-daha-hızlı (FTN) sinyalleşmesi olarak bilinen dikgen olmayan bir fiziksel katman iletim yaklaşımını benimsemektir. Ancak, FTN sinyalleşme, girişimle başa çıkmak için karmaşıklık getirmektedir. Bu tez, ilk olarak kanal kodlamanın düşük karmaşıklıklı bir FTN algılayıcı üzerindeki etkisini incelemektedir. Kanal kodlaması, ikili ve ikili olmayan düşük yoğunluklu eşlik kontrol kodları ile kutupsal kodları altında yapılmaktadır. Benzetim sonuçları, kanal kodlamasının FTN algılayıcı ile en iyi BCJR algılayıcı arasındaki performans farkını azaltmada etkili olduğunu göstermektedir. Dolayısıyla, hızlandırma veya paketleme parametresi olarak adlandırılan τ'nun özellikle yüksek değerleri için, yüksek karmaşıklığa sahip bir FTN algılayıcıya kesin bir ihtiyaç olmadığını göstermektedir. Ek olarak, tez, koordinat serpiştirmeli FTN sinyalleşmesi tekniğini tanıtarak bu temelde düşük karmaşıklıklı bir FTN algılayıcı tasarlayıp mevcut literatürle karşılaştırmaktadır. Bu yenilikçi yaklaşım, 0.6 dB gibi nisbeten az bir maliyetle, %10 spektral verimlilik (SE) artışı sağlarken, performans ile karmaşıklık arasında olumlu bir denge kurmaktadır. Ayrıca, tez FTN sinyalleşmesi algılama sorununu bir yarıkesin problem olarak ele alıp M-PAM için arabul çizelgesi destekli düşük karmaşıklıklı yumuşak çıktılı yarıkesin rahatlama (SDR) tabanlı bir algılayıcı önermektedir. Benzetim sonuçları, bu algılayıcının, polinom hesaplama karmaşıklığına sahip ve daha yüksek kipleme şemalarına uyum sağlayabilen bir yapısı ile 4-PAM için kodlu BCJR performansına 0.8 dB'ye kadar yaklaştığını göstermektedir. Bununla beraber, SNR tabanlı arabul çizelgeleri kullanıldığında performansta 0.3 dB'lik bir iyileşme elde edilmektedir. Düşük karmaşıklık doğası göz önüne alındığında, bu, yumuşak çıkışlı SDR algılayıcının, üretilen log-olabilirlik oranları (LLR'ler) açısından yüksek kipleme için iyi bir performans sağlayabileceğini göstermektedir.

Anahtar kelimeler: Nyquist'ten-daha-hızlı sinyalleşme, kanal kodlama, yarı kesin gevşetme, ortogonal olmayan fiziksel katman iletim tekniği, dışbükey optimizasyon.

CONTENTS

NOMENCLATURE

Roman Letter Symbols

G	Inter-Symbol Interference Matrix
K	Length of Message Sequence
L	Length of Inter-Symbol Interference
N	Length of Codeword Sequence
T	Symbol Period, s
W	Bandwidth, Hz

Greek Letter Symbols

α	Rolloff factor
λ	Log-likelihood Value
μ	Mean
Σ	Covariance
σ^2	Variance
τ	Accelaration/Packaging Parameter

Subscripts

av	Average
I	Inphase Component
Q	Quadrature Component
s	Symbol

Acronyms

APP	A-Posterirori Probability
AWGN	Additive White Gaussian Noise
BCJR	Bahl-Cocke-Jelinek-Raviv
BER	Bit Error Rate
BPSK	Binary Phase Shift Keying
CI-FTN	Coordinate Interleaved Faster-than-Nyquist
FDE	Freqeuncy Domain Equalization
FTN	Faster-than-Nyquist
GF	Galois Field
ISI	Intersymbol Interference

LLR	Log-Likelihood Ratio
LUT	Look-Up Table
M-PAM	Pulse Amplitude Modulation
M-QAM	M-ary Quadrature Amplitude Modulation
MAP	Maximum A-Posterirori Probability
MIMO	Multiple Input Multiple Output
MLSE	Maximum Likelihood Sequence Estimation
MMSE	Minimum Mean Square Error
NB-LDPC	Non-Binary Low Density Parity Check
NOMA	Non-Orthogonal Multiple Access
PCM	Parity Check Matrix
PDA	Probabilistic Data Association
PR	Partial Response
QPSK	Quadrature Phase Shift Keying
SCD	Successive Cancellation Decoding
SDR	Semidefinite Relaxation
SE	Spectral Efficiency, $bits/s/Hz$
soSDR	Soft Output Semidefinite relaxation
SSSgbKSE	Successive Symbol by Symbol go back K Sequence Estimation
SVD	Singular Value Decomposition
VA	Viterbi Algorithm

LIST OF TABLES

LIST OF FIGURES

CHAPTER 1

INTRODUCTION

1.1 Physical Layer Transmission Techniques

Prior to delving into faster-than-Nyquist (FTN) signaling, this section elucidates the concepts of Nyquist signaling and Partial Response signaling as transmission techniques. Understanding these foundational techniques will facilitate a clearer comprehension of FTN signaling.

1.1.1 Nyquist signaling

When considering a digital communication system, it comprises a transmit filter denoted as $G_t(f)$, a receive filter denoted as $G_r(f)$, and a channel represented by $H(f)$, with $|f| < W$, where f is the frequency variable and W is the null-to-null bandwidth. The receiver's output can be expressed as follows:

$$X(f) = G_r(f) \cdot G_r(f) \cdot H(f). \tag{1.1}$$

Upon sampling the signal $x(t)$, the inverse fourier transform of $X(f)$, at $t = mT$, where $m = \ldots, -2, -1, 0, 1, 2$ and T represents the symbol interval, we obtain the desired symbol $x(0)$ along with interference $x(mT)$ from other symbols at $m \neq 0$. At this juncture, our objective is to eliminate Intersymbol Interference (ISI). The initial efforts to address this concern were pioneered by Nyquist, leading to what is known as the Nyquist pulse shaping criterion. In the frequency domain, this criterion translates to the requirement that $X(f)$ must adhere to the following condition:

$$\sum_{m=-\infty}^{\infty} X\left(f + \frac{m}{T}\right) = T. \tag{1.2}$$

One scenario satisfies Equation **1.2**, corresponding to zero Inter-Symbol Interference (ISI) when $\frac{1}{T} = 2W$, a condition known as the Nyquist rate. In simpler terms, the Nyquist rate represents the maximum achievable transmission rate and aligns with the utilization of the sinc pulse. However, opting for the sinc pulse introduces challenges

due to its vulnerability to infinite ISI components caused by timing errors in sampling, rendering it impractical.

As a result, communication predominantly occurs under the condition $\frac{1}{T} < 2W$, where the raised cosine filter has gained widespread adoption as the symbol pulse. The impulse and frequency responses of the raised cosine filter are depicted in Figure 1.1 and Figure 1.2, respectively. This filter has become the symbol pulse of choice due to its practicality. As the roll-off factor α increases, the attenuation of side lobes

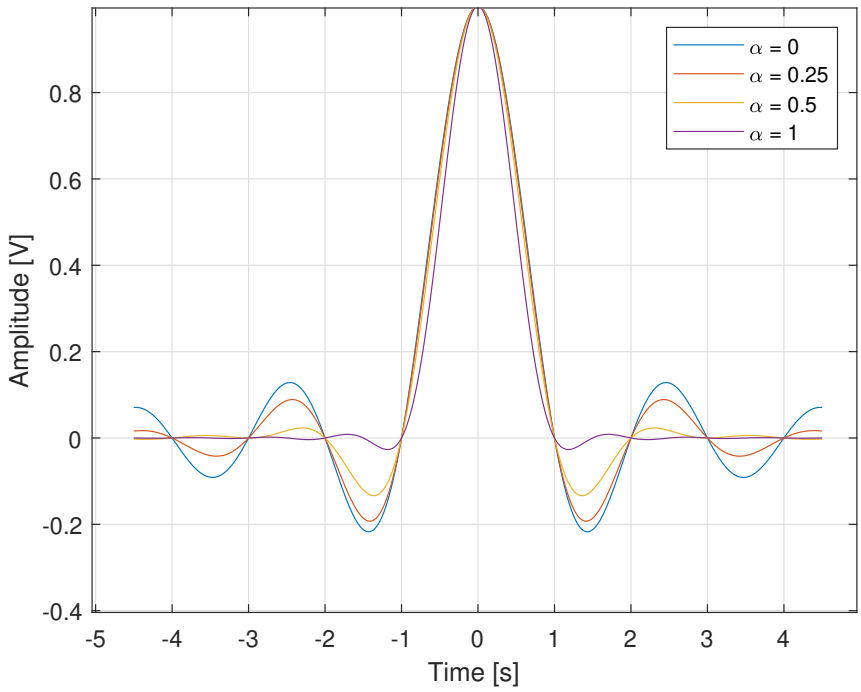

Figure 1.1 Impulse response of raise cosine filter for different values of roll-off factor(α)

becomes more pronounced. This, in turn, necessitates the utilization of greater excess bandwidth, given by $\frac{\alpha}{2T}$. When examining the null-to-null bandwidth W, it becomes evident that employing this excess bandwidth leads to a reduction in spectral efficiency as seen from Equation **1.3**.

$$SE_{NYQ} = \frac{Rb_{NYQ}\log_2 M}{W_{3dB}(1+\alpha)}, \tag{1.3}$$

where M is the number of levels possible with m bits; i.e, $m = \log_2 M$, and

$$Rb_{NYQ} = \frac{1}{T}, \tag{1.4}$$

which is called the Nyquist bit rate that is equal to $2W_{3dB}$.

$$W = W_{3dB}(1+\alpha). \tag{1.5}$$

Please note that, in accordance with the Nyquist criterion, we can transmit symbols at the maximum rate of $2W_{3dB}$ when employing a raised cosine filter.

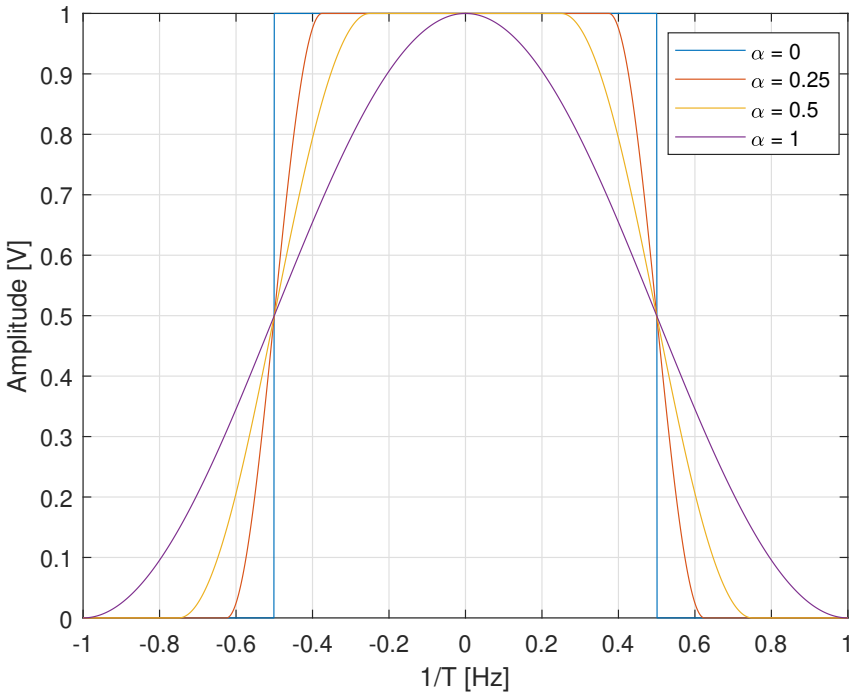

Figure 1.2 Frequency response of raised cosine filter for various values of roll-off factor(α)

1.1.2 Partial Response Signaling

As previously discussed, it is necessary to operate below $2W$ for achieving a zero Inter-Symbol Interference (ISI) condition. Attaining the Nyquist rate of $2W$ symbols/s presents two potential approaches: relaxing the bandwidth, which reduces spectral efficiency due to excess bandwidth, or introducing controlled ISI into the system through the design of a pulse shape denoted as $X(f)$. Partial Response (PR) signaling is one technique that employs controlled ISI. Within PR signaling, various schemes exist. An illustrative scheme, susceptible to ISI only from its immediate neighboring symbols, is presented in Equation **1.6**. Notably, the pulse shape $X(f)$ in this scheme does not

adhere to the Nyquist criterion, leading to the presence of ISI.

$$\sum_{m=-\infty}^{\infty} X(f+\frac{m}{T}) = T + T\exp(-j2\pi fT). \tag{1.6}$$

However, the waveform $x(t)$ illustrated in Figure 1.3, which corresponds to Equation **1.7**, can achieve a value of $T = \frac{1}{2W}$ while encountering Inter-Symbol Interference (ISI) exclusively from the symbol immediately adjacent to its right. A more comprehensive understanding of the frequency domain characteristics of $x(t)$, represented by $X(f)$, is elucidated in Figure 1.4.

$$x(t) = \text{sinc}(t) + \text{sinc}(t-T). \tag{1.7}$$

Binary PR signals were initially introduced by [1]. Subsequently, researchers delved into the realm of optimal transmit and receiver filters, with studies conducted by [2–4]. Further advancements emerged as Forney and Omura explored the utilization of the Viterbi algorithm for the detection of PR signals in their works [5, 6].

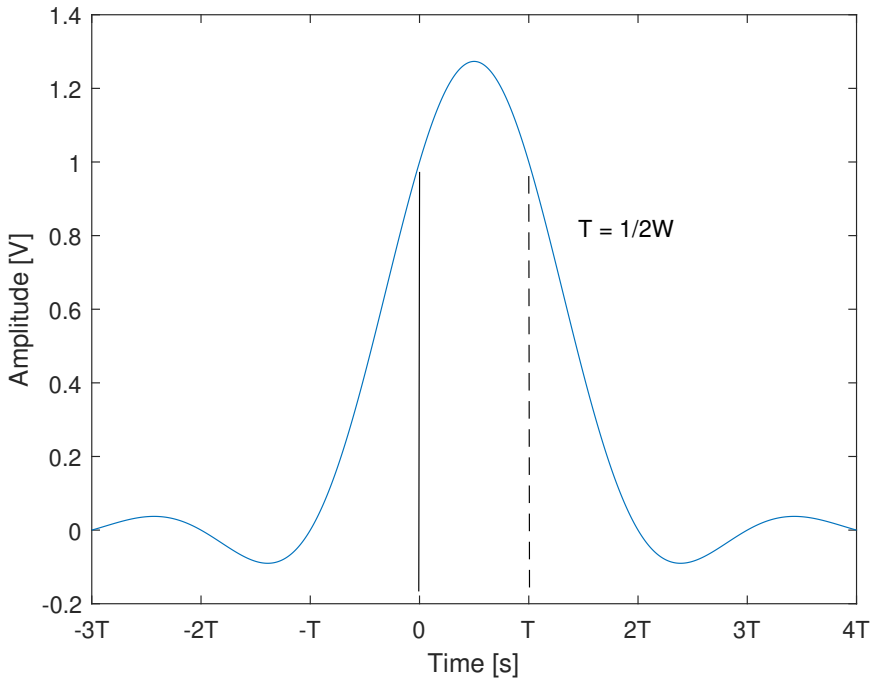

Figure 1.3 Time-domain characteristics of a PR signal

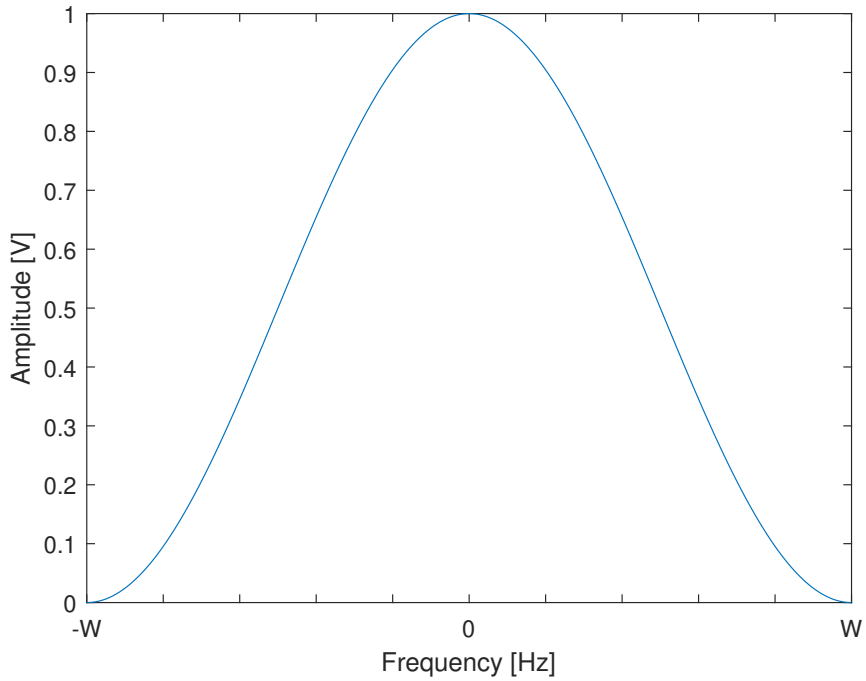

Figure 1.4 Frequency-domain characteristics of a PR signal

1.1.3 Faster-than-Nyquist signaling

Faster-than-Nyquist (FTN) signaling, as the name suggests, departs from conventional Nyquist signaling to achieve enhanced spectral efficiency within the same bandwidth and energy constraints. In essence, FTN signaling transmits symbols at a rate exceeding the Nyquist rate;i.e, $\frac{1}{T} > 2W_{3dB}$, deliberately introducing Inter-Symbol Interference (ISI) akin to Partial Response (PR) signaling. The pioneering work of Mazo in [7] revealed that using a sinc pulse, the minimum distance between symbols remains constant at the rate of $\frac{1}{\tau T}$, $\tau \in [0.8021]$, leading to the recognition of $\tau = 0.802$ as the Mazo limit. It's important to note that the Mazo limit varies with the roll-off factor, which characterizes the excess bandwidth that the FTN signaling employs more efficient than Nyquist signaling (Equation **1.8**).

$$SE_{FTN} = \frac{Rb_{FTN}\log_2 M}{W_{3dB}(1+\alpha)}, \tag{**1.8**}$$

where $Rb_{FTN} = 1/\tau T$. The FTN signaling framework can be expressed using

$$s(t) = \sum_n a_n h(t - n\tau T), \tag{**1.9**}$$

where a_n represents the transmit symbol, and $h(t)$ denotes the pulse shaping filter. The received signal is given by

$$y(t) = \sum_{n=1}^{N} a_n g(t - n\tau T) + w(t), \tag{1.10}$$

with $g(t) = \int h(x)h(x-t)dx$ and $w(t) = \int n(x)h(x-t)dx$. The sampler output can be elegantly represented in matrix form as

$$\mathbf{y} = \mathbf{Ga} + \mathbf{w}, \tag{1.11}$$

where **G** is the ISI matrix, taking the form of

$$\mathbf{G} = \begin{bmatrix} G_{1,1} & G_{1,2} & G_{1,3} & \cdots & G_{1,L} & 0 & 0 & 0 & 0 & 0 \\ G_{1,2} & G_{1,1} & G_{1,2} & G_{1,3} & \cdots & G_{1,L} & 0 & 0 & 0 & 0 \\ G_{1,3} & G_{1,2} & G_{1,1} & G_{1,2} & G_{1,3} & \cdots & G_{1,L} & 0 & 0 & 0 \\ \vdots & \vdots & \vdots & \vdots & \vdots & \vdots & \vdots & \vdots & \vdots & \vdots \\ \cdots & \cdots & G_{1,3} & G_{1,2} & G_{1,1} & G_{1,2} & G_{1,3} & \cdots & \cdots & \cdots \\ \vdots & \vdots & \vdots & \vdots & \vdots & \vdots & \vdots & \vdots & \vdots & \vdots \\ 0 & 0 & 0 & G_{1,L} & \cdots & G_{1,3} & G_{1,2} & G_{1,1} & G_{1,2} & G_{1,3} \\ 0 & 0 & 0 & 0 & G_{1,L} & \cdots & G_{1,3} & G_{1,2} & G_{1,1} & G_{1,2} \\ 0 & 0 & 0 & 0 & 0 & G_{1,L} & \cdots & G_{1,3} & G_{1,2} & G_{1,1} \end{bmatrix}. \tag{1.12}$$

From this matrix, it is apparent that symbols at the receiver are impacted by intersymbol interference (ISI) originating from the L preceding and succeeding symbols. Additionally, it is clear that **Ga** results from the processes of pulse shaping, matched filtering, and sampling.

Incorporating FTN signaling introduces the phenomenon of Inter-Symbol Interference (ISI), which adds a layer of complexity to the process of signal detection. As a result, it becomes necessary to apply equalization techniques in order to accurately detect the transmitted symbols. An effective strategy for detecting FTN signals involves the utilization of both the Viterbi algorithm (VA) and the Bahl-Cocke-Jelinek-Raviv (BCJR) algorithm [8]. Nevertheless, these advanced detectors exhibit a level of complexity that

grows exponentially. To address the challenge posed by the intricate equalization complexity, previous research efforts, as documented in works like [9] and [10], have introduced truncated versions of the VA algorithm and BCJR algorithm, which operate with simplified state configurations. While these algorithms showcase exceptional performance in scenarios where ISI is significant, they also come with a high degree of computational complexity. Strategies for detection with reduced complexity are put forth, as evidenced in sources like [11–14]. The matter of high-order QAM and PSK in the context of FTN signaling is explored in [15] and [12], both characterized by a computational load of approximately $O(N^{3.5})$. In a similar computational realm, the investigation detailed in [16] concentrates on probabilistic data association (PDA) algorithms designed for BPSK FTN signaling. Additionally, a method of iterative detection, entailing a computational complexity of around $O(L)$, is introduced in [17].

All of them shows that it is important to explore alternative strategies that provide a reduction in complexity. Another aspect to consider is that a significant portion of the scholarly attention in reduced-complexity FTN signaling investigations has been directed toward detection algorithms, neglecting their incorporation alongside channel codes. This omission is apparent in cases where reduced-complexity FTN detection algorithms are not included when channel codes are implemented, as observed in references such as [18] and [19]. Alternatively, the employment of the BCJR detection algorithm is noted as another instance of this oversight, as seen in [20, 21].

In the scope of this thesis, our emphasis lies in the design of low-complexity detectors and the interaction between channel coding and low-complexity detection within the FTN signaling framework. Chapter 2 evaluates the impact of channel coding on a low-complexity detector. Chapter 3 introduces a receiver's low-complexity detector alongside a transmitter's precoding-like structure. In Chapter 4, the FTN signaling problem is formulated as a semidefinite problem, leading to the proposal of a soft-output Semi-Definite Relaxation (SDR) based low-complexity detector. The thesis concludes with Chapter , which includes its final remarks and a discussion of future prospects and challenges within the domain of faster-than-Nyquist signaling.

CHAPTER 2

CHANNEL CODED LOW-COMPLEXITY DETECTORS

In this chapter, we assess the performance of a very low complexity Successive Symbol-by-Symbol Go Back K Sequence Estimation (SSSgb$K$SE) detector in a channel-coded environment [22, 23], considering specific key parameters.

2.1 Faster-than-Nyquist Signaling Detectors and Channel Codes

The incorporation of channel codes and their impact on low-complexity FTN signaling detection algorithms has received limited attention in the existing literature. Prevailing studies often either focus on utilizing the BCJR detection algorithm in the presence of a channel code or neglect to account for reduced complexity FTN detection algorithms altogether. The exploration of channel coded methodologies is crucial, as they may offer a more fitting solution for FTN signaling, particularly at specific τ values.

2.1.1 Successive Symbol-by-Symbol Go Back K Algorithm

While Nyquist signaling allows for independent symbol-by-symbol detection, the situation contrasts with FTN signaling. In the latter, isolating the detection of a single symbol, without considering the rest, results in performance degradation due to Intersymbol Interference (ISI). This arises from the dependency between the symbols.

This interdependence becomes conspicuous when inspecting the sampled output of the matched filter at time τT, as illustrated below:

$$\begin{aligned} y_k &= y(k\tau T) \\ &= \sqrt{E_s}\sum_{n=1}^{N} a_n g(k\tau T - n\tau T) + w(k\tau T) \\ &= \underbrace{\sqrt{E_s}a_k g(0)}_{\text{desired symbol}} + \underbrace{\sqrt{E_s}\sum_{n=1,n\neq k}^{N} a_n g((k-n)\tau T)}_{\text{ISI from adjacent symbols}} + w(k\tau T), \end{aligned} \tag{2.1}$$

where a_k represents the symbol at time k, while E_s signifies the symbol energy. Consequently, it becomes imperative to consider neighboring symbols and strive for accurate estimation of these symbols.

As demonstrated in Equation **2.2**, directly estimating a symbol in the presence of impending intersymbol interference (ISI) can lead to error propagation, wherein errors in past estimated symbols are carried forward.

$$\hat{a}_k = y_k - \underbrace{G_{1,L}\hat{a}_{k-L+1}...G_{1,2}\hat{a}_{k-1}}_{\text{ISI from previous } L-1 \text{ data symbols}} . \tag{2.2}$$

The study in [17] introduces a novel symbol-by-symbol detector that employs a minimalist approach, involving low-complexity operations and retrospective analysis. By incorporating a backward-oriented methodology, the detector aims to mitigate error propagation and enhance symbol estimation accuracy. The methodology is outlined as follows:

$$\begin{aligned}\hat{\hat{a}}_k = (&y_k \\ &\underbrace{-(G_{1,L}\hat{a}_{k-L+1} + ... + \underbrace{G_{1,K+1}\hat{\hat{a}}_{k-K} + ... + G_{1,2}\hat{\hat{a}}_{k-1})}_{\substack{\text{ISI from previous } K \text{ data symbols} \\ \text{with improved estimation accuracy}}})}_{\text{ISI from previous } L-1 \text{ data symbols}},\end{aligned} \tag{2.3}$$

where G is the ISI matrix and L is the ISI length. For the kth symbol, the algorithm goes back to the $k-K$ and recalculates the estimate for the $k-K$th symbol, taking into consideration both upcoming symbols ($k-K+1$, $k-K+2$, ..., $k-1$, k) and past symbols ($k-K-1$, $k-K-2$, ..., $k-K-L-1$, $k-K-L$). This estimation process is similarly applied for symbols $k-K+1$, $k-K+2$, ..., $k-1$, k. Finally, the re-estimation of a_k involves subtracting the intersymbol interference (ISI) effect originating from the previously re-estimated symbols as in Equation **2.3**.

2.1.2 Viterbi Algorithm

In 1967, A. J. Forney introduced the Viterbi algorithm. However, it was in 1973 that Forney himself recognized and presented an even more efficient version of the Viterbi algorithm. The algorithm aims to identify the optimal transmit sequence or

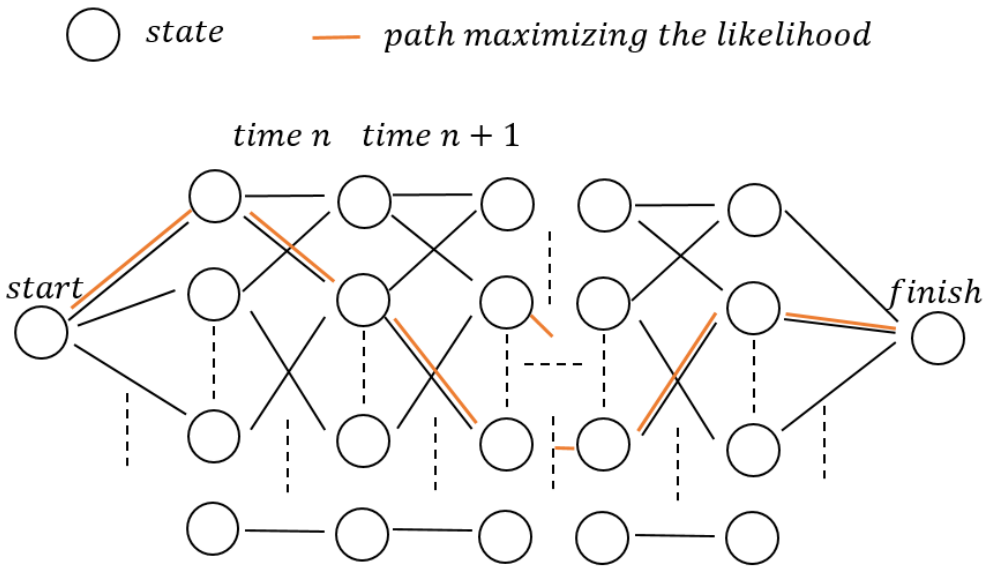

Figure 2.1 Demonstration of Viterbi algorithm

path (Figure 2.1) that maximizes the likelihood $p(r|c)$ through an exhaustive search across the entire codeword sequence set. As a consequence of this comprehensive search, the algorithm's complexity scales proportionally with M^N, where M denotes the modulation level.

2.1.3 BCJR Algorithm

In our pursuit of minimizing bit errors, it becomes imperative to maximize the a posteriori probability (APP), denoted as $p(u_l|r)$. The algorithm that accomplishes this objective, recognized as the Maximum A Posteriori Probability (MAP) decoder, was first introduced in 1974 by Bahl, Cocke, Jelinek, and Raviv, collectively known as BCJR. This algorithm serves to decode a broad spectrum of linear codes, encompassing both convolutional and block codes.

Initially, the popularity of the BCJR algorithm, also referred to as the Bahl-Cocke-Jelinek-Raviv algorithm, was somewhat limited in the 1970s due to its considerably higher complexity when compared to the Viterbi algorithm. However, the landscape shifted in the 1990s with the emergence of turbo codes and concatenated codes, which necessitated the extraction of soft output. This shift led to a resurgence in the algorithm's popularity in subsequent years.

The BCJR algorithm calculates a crucial metric called the log-likelihood (L-value) for

each bit. Specifically, the L-value $L(u_l)$ for the l-th input bit or the input bit at time l is computed as follows:

$$L(u_l) = \log\left(\frac{p(u_l = +1|r)}{p(u_l = -1|r)}\right). \tag{2.4}$$

Using Bayes theorem, the APP value $p(u_l = +1|r)$ is written as

$$p(u_l = +1|r) = \log\left(\frac{p(u_l = +1, r)}{p(r)}\right) \quad = \frac{\Sigma_{u \in U_l^+} p(r|c)P(u)}{\Sigma_u p(r|c)P(u)}, \tag{2.5}$$

where c is the encoded data. where U_l^+ is the set of input sequences such that $u_l = +1$. Similarly we get the probability of u_l being -1 as

$$p(u_l = -1|r) = \log\left(\frac{p(u_l = -1, r)}{p(r)}\right) \quad = \frac{\Sigma_{u \in U_l^-} p(r|c)P(u)}{\Sigma_u p(r|c)P(u)}. \tag{2.6}$$

Continuing from where you left off, the expression for the L-value of the input bit at time l is expressed as

$$L(u_l) = \log\left(\frac{\Sigma_{u \in U_l^-} p(r|c)P(u)}{\Sigma_{u \in U_l^-} p(r|c)P(u)}\right). \tag{2.7}$$

Upon further analysis of Equation **2.5**, it can be re-expressed as

$$p(u_l = +1|r) = \frac{\Sigma_{(s',s) \in \Sigma_l^+} p(s', s, r)}{p(r)}. \tag{2.8}$$

In this equation, Σ_l^+ refers to the set of state pairs s' and s at time l and $l+1$, respectively. These state transitions exclusively involve the input bit $u_l = +1$. When evaluating the joint probability density function $p(s', s, r)$ in Equation **2.8** for $r_{t<l}$, r_l, and $r_{t>l}$, it simplifies to

$$\begin{aligned} p(s', s, r) &= p(s', s, r_{t<l}, r_l, r_{t>l}) \\ &= p(r_{t>l}|s', s, r_{t<l}, r_l)p(s', s, r_{t<l}, r_l) \\ &= p(r_{t>l}|s', s, r_{t<l}, r_l)p(r_l, s|r_{t<l}, s')p(r_{t<l}, s') \\ &= p(r_{t>l}|s)p(r_l, s|s')p(r_{t<l}, s') \\ &= \beta_{l+1}(s)\gamma(s, s')\alpha_l(s'), \end{aligned} \tag{2.9}$$

where $\beta_{l+1}(s) = p(r_{t>l}|s)$, $\gamma(s, s') = p(r_l, s|s')$, and $\alpha_l(s') = p(r_{t<l}, s')$.

In essence, the BCJR algorithm derives the Maximum A Posteriori (MAP) estimation by modeling the problem using a trellis structure, as depicted in Figure 2.2. In the

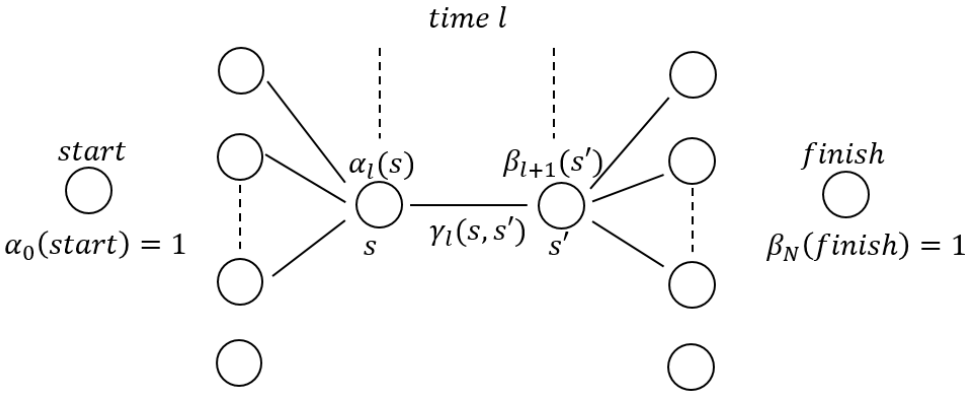

Figure 2.2 Demonstration of BCJR algorithm

context of employing the BCJR algorithm for FTN signaling as an FTN detector, it is noteworthy that the Intersymbol Interference (ISI) length parallels the concept of memory length in convolutional coding. Consequently, the complexity of the detector undergoes an exponential increase due to this correspondence.

An alternative approach, known as M-BCJR algorithm [20], offers a reduction in complexity compared to the standard BCJR algorithm. The M-BCJR algorithm operates similarly to BCJR, with the notable difference being the selection of the M α and β branch metrics featuring the highest probabilities. This strategic selection serves to curtail complexity while maintaining an effective decoding process.

2.1.4 Channel Codes

To achieve or come close to the coveted Shannon capacity, which guarantees reliable communication amidst noise and interference, the utilization of Forward Error Correction (FEC) mechanisms is of paramount significance. This technique becomes our ally in achieving robust data transfer. Notably, some promising error correction codes have emerged as beacons of efficiency. Among these, Non-Binary Low-Density Parity Check (NB-LDPC) codes shine for their ability to deliver commendable performance with shorter codeword lengths compared to conventional LDPC codes. On a similar note, Polar codes have garnered attention for their strategic deployment –

3rd Generation Partnership Project (3GPP) have chosen Polar codes for control channels and LDPC codes for data channels. This selection is complemented by the incorporation of Faster-Than-Nyquist (FTN) signaling. Here, we briefly delve into these developments:

2.1.4.1 Polar Codes

In 2009, Arikan [24] introduced Polar codes, revolutionizing the landscape by transforming N independent channels into N novel abstract channels, characterized by varying levels of reliability. This transformation process, termed Polarization, yields a mixture of reliable and unreliable channels. This polarization unfolds through two pivotal stages: Channel combining, where new channels with W capacity emerge from independent channels, and splitting, which defines the bit-level impact post-combining.

During encoding, the inputs undergo transformation using a generator matrix G. However, an essential pre-encoding step involves allocating transmit bits to predetermined, reliable channel indices. This process, known as Polar codes construction, hinges on the determination of new bit channel capacities—reliable channel indices are ascertained using methods such as density evolution.

Finally, channel decoding comes into play. Employing algorithms like the successive cancellation algorithm, we decode channel outputs since these outputs are intricately linked to certain inputs.

In summary, polar codes offer a paradigm shift in channel coding by harnessing the concept of polarization. This technique optimizes the reliability of certain channels while gracefully accommodating channels of varying quality, contributing to enhanced communication efficiency and resilience.

2.1.4.2 Low Density Parity Check Codes

LDPC codes belong to a class of linear error-correcting codes renowned for their sparsely populated parity-check matrices. Decoding these codes is often accomplished through the application of message passing techniques, leveraging the

underlying Tanner graph structure.

Of significant import within graph theory is the notion of cycles – closed paths originating and terminating at the same node. For bipartite graphs, the shortest cycle comprises four edges. Among the message-passing algorithms, the min-sum method and the sum-product algorithm hold prominence. These algorithms exhibit effective convergence in scenarios where the Tanner graph of the code lacks cycles. Intriguingly, the decoding process maintains convergence even in the presence of cycles within the graph. Notably, improved convergence rates are observed when short cycles are absent. To mitigate the existence of such short cycles, a constraint is established to prevent multiple instances of overlap between any two columns within the H matrix, specifically those of length four.

The LDPC decoding process encompasses two fundamental stages: variable-to-check node processing and check-to-variable node processing. Initially, channel-derived Log-Likelihood Ratio (LLR) values are propagated to the check nodes. In this phase, check nodes execute a soft-input, soft-output decoding process via a single parity check mechanism, excluding the corresponding intrinsic LLR value. Subsequently, these check nodes transmit extrinsic LLR values for each bit back to the variable nodes.

The subsequent phase involves variable nodes engaging in a soft-input, soft-output repetition coding procedure. This process incorporates the initial LLR values, generating novel LLR values that are communicated back to the variable nodes. The iterative decoding process progresses through these steps. Iterations conclude either upon the satisfaction of the syndrome check condition or upon reaching the predefined iteration limit.

2.1.4.3 Non Binary Low Density Parity Check Codes

NB-LDPC codes emerge as an evolution of binary LDPC codes tailored for operation within a Galois Field $GF(q)$. The structure of NB-LDPC codes can also be equivalently expressed using binary LDPC codes and cyclic permutations. The dimension of the parity check matrix for the corresponding binary LDPC codes expands proportionally as each set of m bits aligns with a non-binary element in a Galois Field $GF(q)$, where

$q = 2^m$. The NB-LDPC codes have demonstrated notable effectiveness in reducing bit error rates (BER), particularly when addressing short packet communication scenarios [25, 26]. NB-LDPC encoding takes the input sequence $\boldsymbol{u}$ comprising K elements and generates an output sequence $\boldsymbol{x}$ of length N, introducing an increment of M elements. The encoder's output satisfies all the parity check equations stipulated in Equation **2.10**:

$$f_i = \sum_{j=1}^{N_H} H_{i,j} x_j, \qquad H_{i,j} \in GF(q), \tag{2.10}$$

In this context, f_i represents the ith parity check equation. The computational complexity of NB-LDPC decoding poses a challenge. In essence, while achieving robust performance for short block lengths, there's a trade-off involving complexity. The study presented in [27] introduces a viable solution in the form of the Extended Min Sum (EMS) algorithm. This is in response to the significant computational demands introduced by the belief propagation (BP) decoding process. The EMS algorithm strategically employs only the n_m most reliable probabilities during each iteration, where $n_m \ll q$. Consequently, it effectively reduces the decoding complexity from $O(q^2)$ associated with the BP decoder to $O(n_m \log_2 n_m)$. To counter this challenge, the EMS algorithm has been devised as a low-complexity decoding methodology tailored for NB-LDPC codes. It proves particularly well-suited for scenarios involving short packet communications, as highlighted in [25], where minimal latency is a requirement. The EMS decoder operates on the basis of log-likelihood ratios (LLRs). Each codeword symbol's LLR vector is represented as

$$\boldsymbol{\ell}(z) = \begin{bmatrix} \ell_0 & \ell_1 & \dots & \ell_{q-1} \end{bmatrix}^T, \tag{2.11}$$

and the likelihood of a message α_i is defined by

$$\ell_i = \log \frac{P(z = \alpha_i)}{P(z = \alpha_0)}, \qquad i \in \{0, \dots, q-1\}, \tag{2.12}$$

where z denotes a connection within the Tanner graph, and $\ell_(z)$ signifies the likelihoods associated with that connection. The structure of the NB-LDPC codes relies on iterative decoders, wherein a decoder iteration encompasses the

determination of variable-to-check (V2C) messages, check-to-variable (C2V) messages, and a syndrome check. The EMS decoder terminates either upon fulfillment of all syndromes or upon reaching a predefined iteration limit.

2.2 System Model

We use the system model in Figure 2.3 to get the performance of different coded scenarios. Message bits generated is encoded by channel encoder at the given code rate $\frac{K}{N}$. Encoded message bits are mapped to the corresponding symbols of the binary phase shift keying (BPSK) modulation constellation.

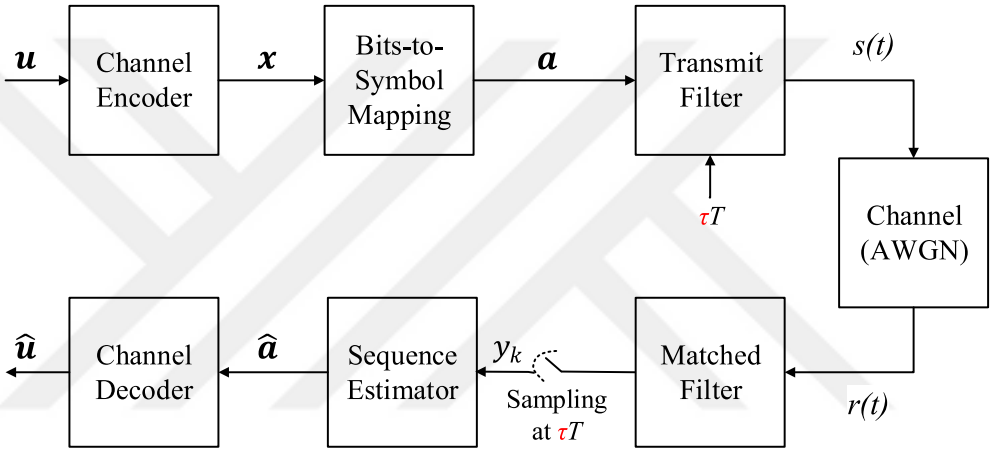

Figure 2.3 Channel coded system model for FTN signaling.

The symbols are shaped by the root raised cosine filter $p(t)$, i.e, pulse shaping filter, to be transmitted at the rate of $\frac{1}{\tau T}$.

$$s(t) = \sqrt{E_s \frac{K}{N}} \sum_{n=1}^{N} a_n h(t - n\tau T), \quad 0 < \tau \leq 1, \tag{2.13}$$

where E_s is the symbol energy. The transmit signal passes through the channel and we get the received signal as

$$r(t) = s(t) + n(t). \tag{2.14}$$

Then the received signal corrupted by both channel and FTN signaling is matched to

the matched filter to get the maximum signal-to-noise ratio as follows:

$$\begin{aligned} y(t) &= \int_{-\infty}^{\infty} s(\gamma)h(t-\gamma)d\gamma + \int_{-\infty}^{\infty} n(\gamma)h(t-\gamma)d\gamma \\ &= \int_{-\infty}^{\infty} \sqrt{E_s\frac{K}{N}} \sum_{n=1}^{N} a_n h(\gamma - n\tau T)h(t-\gamma)d\gamma + \int_{-\infty}^{\infty} n(\gamma)h(t-\gamma)d\gamma \\ &= \int_{-\infty}^{\infty} \sqrt{E_s\frac{K}{N}} \sum_{n=1}^{N} a_n h(\gamma - n\tau T)h(\gamma-t)d\gamma + \int_{-\infty}^{\infty} n(\gamma)h(\gamma-t)d\gamma. \end{aligned} \tag{2.15}$$

The received signal passing the matched filter is sampled at every τT as

$$\begin{aligned} y(k\tau T) &= \int_{-\infty}^{\infty} \sqrt{E_s\frac{K}{N}} \sum_{n=1}^{N} a_n h(\gamma - n\tau T)h(\gamma - k\tau T)d\gamma \\ &\quad + \int_{-\infty}^{\infty} n(\gamma)h(\gamma - k\tau T)d\gamma \\ &= \int_{-\infty}^{\infty} \sqrt{E_s\frac{K}{N}} \sum_{n=1}^{N} a_n g(n\tau T - k\tau T)d\gamma + \int_{-\infty}^{\infty} w(k\tau T)d\gamma \\ &= \sqrt{E_s\frac{K}{N}} \sum_{n=1}^{N} a_n g(n\tau T - k\tau T) + w(k\tau T). \end{aligned} \tag{2.16}$$

Please notice that there is no orthogonality between the noise samples anymore. The sampled symbols are estimated by the FTN detector, SSSgbKSE based on the symbol. Normally, after the estimator or detector block there is also need for a soft demapper block, but as we use the BPSK modulation in this work and thus consider detector output as log-likelihood ratio(LLR) it is not involved here. Lastly, the output of the detector goes as initial log-likelihood(LLR) directly into channel decoder which tries to find the correct transmit message bits.

2.3 Simulation Results for Polar Coded SSSgbKSE FTN Detector

A simulation of the FTN system employing polar codes is executed through the SSSgb*K*SE detection technique, followed by a comparison of its efficacy with that of the BCJR algorithm. The study delves into an examination of the system's performance in terms of the bit error rate (BER). This performance assessment is conducted within a framework involving BPSK modulation and the presence of additive white Gaussian noise (AWGN) within the communication channel. The

analysis encompasses the consideration of distinct values for τ, specifically 0.8, 0.7, and 0.6.

During the simulation process, a polar code with a length of $N = 1024$ and a code rate of $1/2$ is employed. The decoding of the polar code is accomplished using a successive cancellation decoding (SCD) algorithm, which exhibits a computational complexity of $O(N\log(N))$. For the transmission phase, a filter is employed that adheres to the attributes of a root raised cosine waveform, characterized by a roll-off factor denoted as $\alpha = 0.3$. Furthermore, for the SSSgb$K$SE algorithm, where the complexity is represented as $O(L)$, a value of $K = 1$ is utilized.

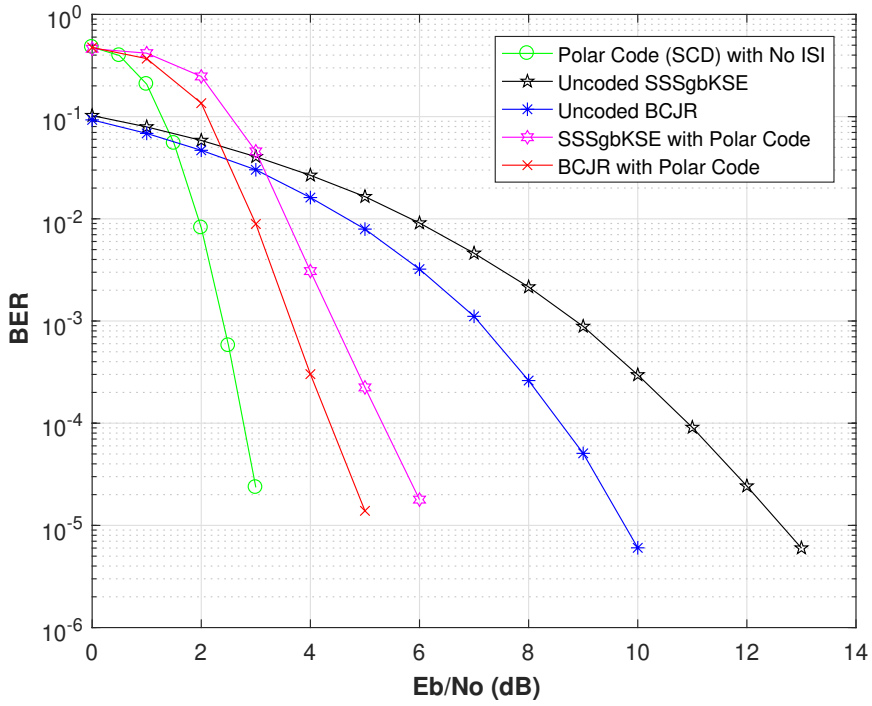

Figure 2.4 Performance comparison at $\tau = 0.8$.

In the context of Figure 2.4, Figure 2.5, and Figure 2.6, it becomes apparent that the optimal FTN detector, the BCJR, approaches the Nyquist signaling by 2 dB. This tendency holds across all τ values at a bit error rate (BER) of 10^{-4}. In exchange for this 2 dB trade-off, the FTN signaling yields significantly higher spectral efficiencies of 25%, 43%, and 66% for $\tau = 0.8$, 0.7, and 0.6 respectively, in comparison to the Nyquist counterpart. At $\tau = 0.8$, when moving from the uncoded scenario to the coded scenario, the gap between the SSSgbKSE and the BCJR reduces from 2.2 dB to 1

dB. This finding underscores the beneficial impact of polar codes in improving the performance of the SSSgbKSE by 1.2 dB.

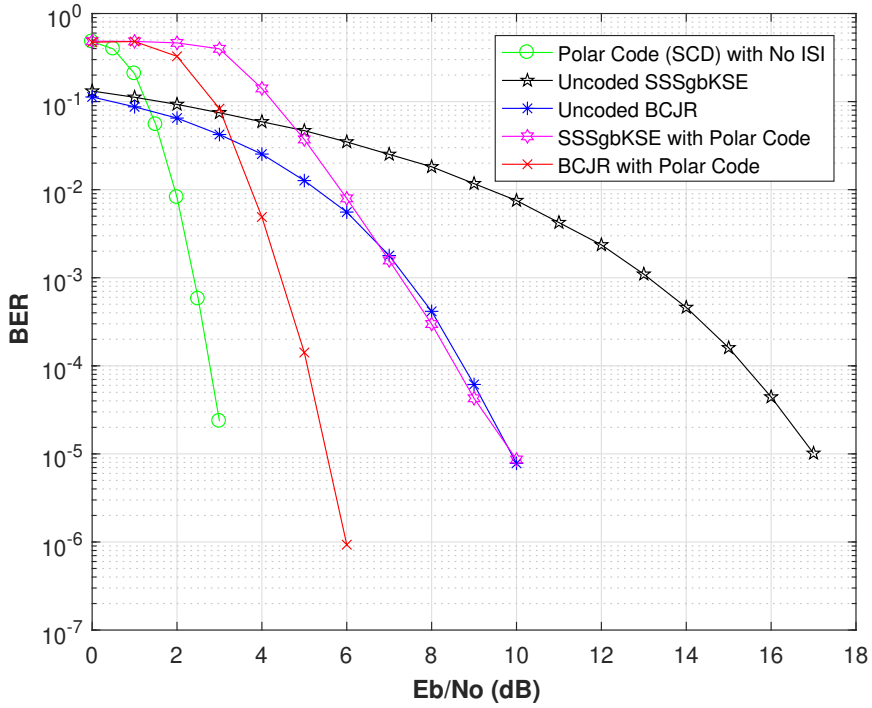

Figure 2.5 Performance comparison at $\tau = 0.7$.

Within Figure 2.5 and Figure 2.6, the impact of intersymbol interference (ISI) becomes notably pronounced as τ experiences a decrease. In the same τ ranges for both scenarios, the BCJR manages to achieve performance equivalent to that at $\tau = 0.8$, but this accomplishment is accompanied by a notable escalation in complexity. Delving into the uncoded scenario, the SSSgbKSE achieves a BER of 10^{-4} but demands higher $\frac{E_b}{N_o}$ values, specifically 6.6 dB and 12 dB. Conversely, in the coded scenario, $\tau = 0.7$ and $\tau = 0.6$ require energy levels of 3.5 dB and 11 dB, respectively. This observation underscores the role of channel coding, which extends its supportive impact to the SSSgbKSE by 3.1 dB at $\tau = 0.7$ and 1 dB at $\tau = 0.6$, a juncture where the reliability of LLR experiences further attenuation.

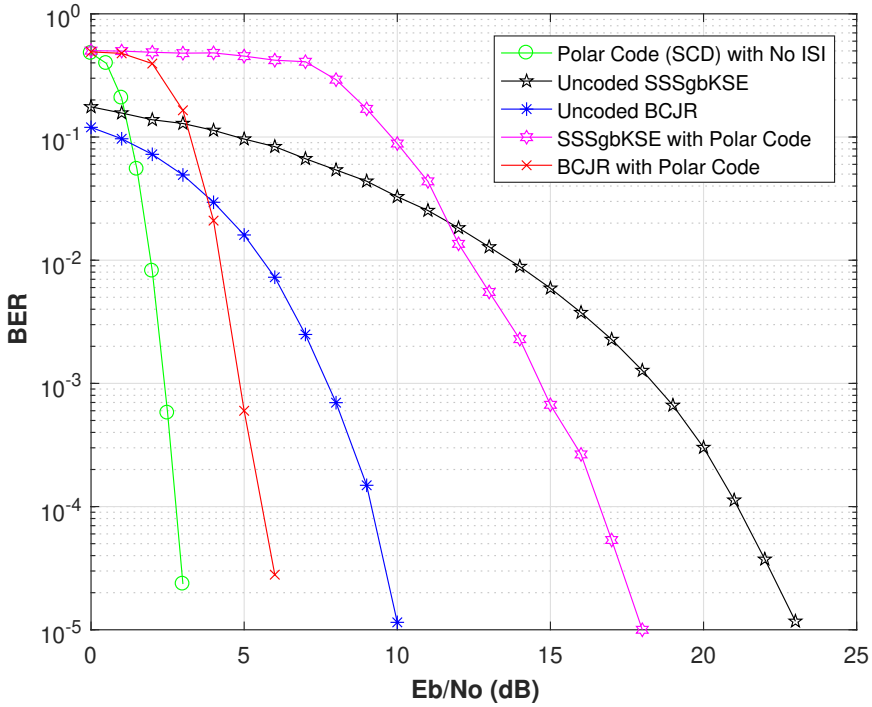

Figure 2.6 Performance comparison at $\tau = 0.6$.

2.4 Simulation Results for NB-LDPC Coded SSSgbKSE FTN Detector

In this section, our primary focus revolves around conducting an exploration of the performance facets associated with the transmission of coded BPSK FTN signaling. Specifically, our investigation delves into scenarios involving LDPC(N,K) and NB-LDPC(N,K) codes, with careful consideration of time acceleration parameters at values of 0.8 and 0.9. Our study encompasses the utilization of the M-BCJR algorithm for $M = 32$, alongside the SSSgb$K$SE algorithm with $K = 1$.

For the case of a code rate of 0.5, we employ NB-LDPC codes such as NB-LDPC(120,60), NB-LDPC(264,132), and NB-LDPC(504, 252), ensuring that the codeword length is a multiple of 12 to match the usage of $GF(2^6)$ in NB-LDPC. These NB-LDPC codes are compared against LDPC codes like LDPC(128,63), LDPC(256,128), and LDPC(512,256) to ensure a fair comparison.

In the EMS decoder utilizing the L-bubble method with $L = 4$, the parameter n_m is set

to 20, and the offset is set at 3.

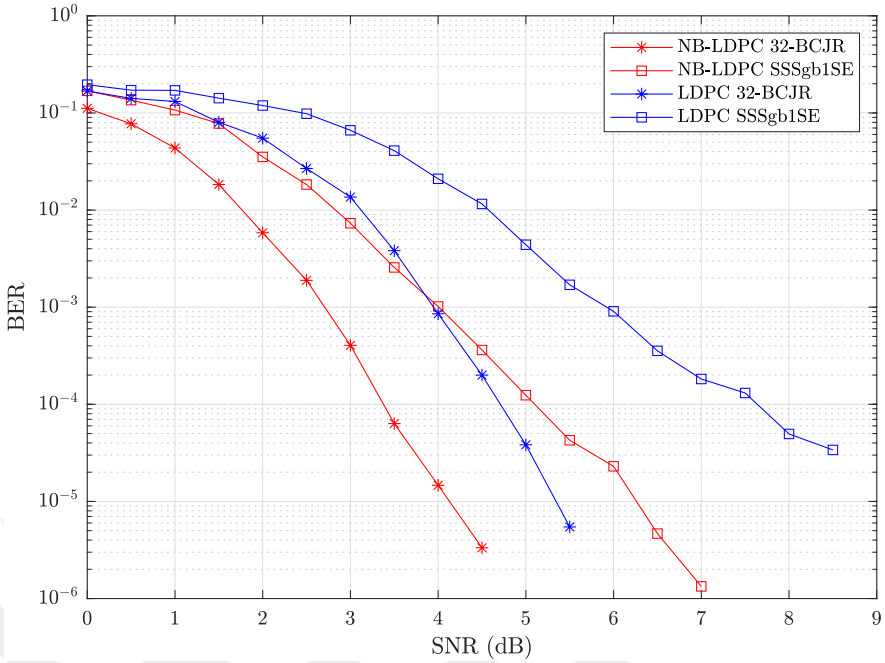

Figure 2.7 BER performance at $\tau = 0.8$, LDPC(128,64), NB-LDPC(120,60)

As anticipated, the performance of NB-LDPC with M-BCJR consistently surpasses that of LDPC with SSSgb$K$SE. Similarly, LDPC with M-BCJR consistently outperforms LDPC with SSSgb$K$SE across all codeword lengths as depicted in Figures 2.7 to 2.12.

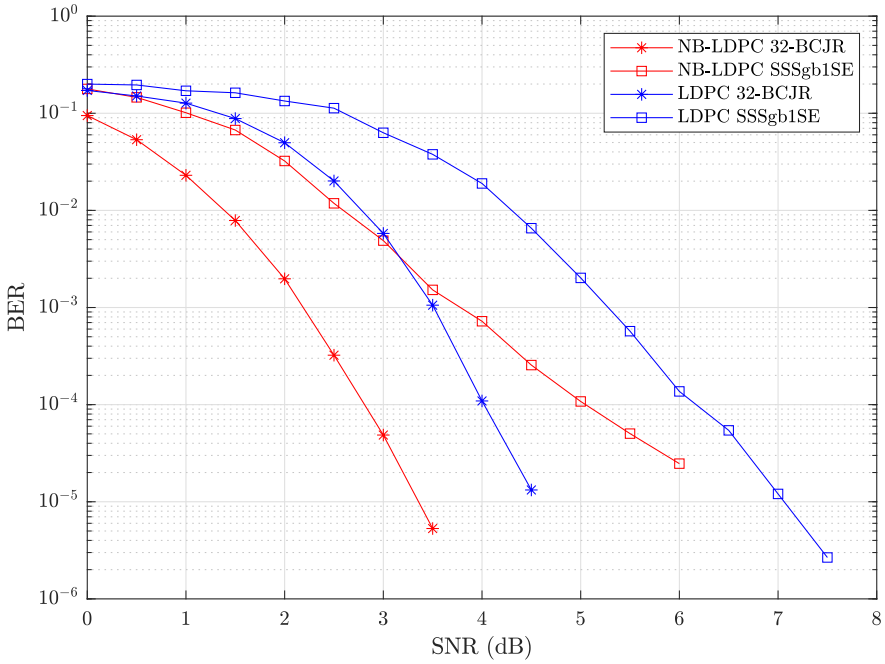

Figure 2.8 BER performance at $\tau = 0.8$, LDPC(256,64), NB-LDPC(264,132)

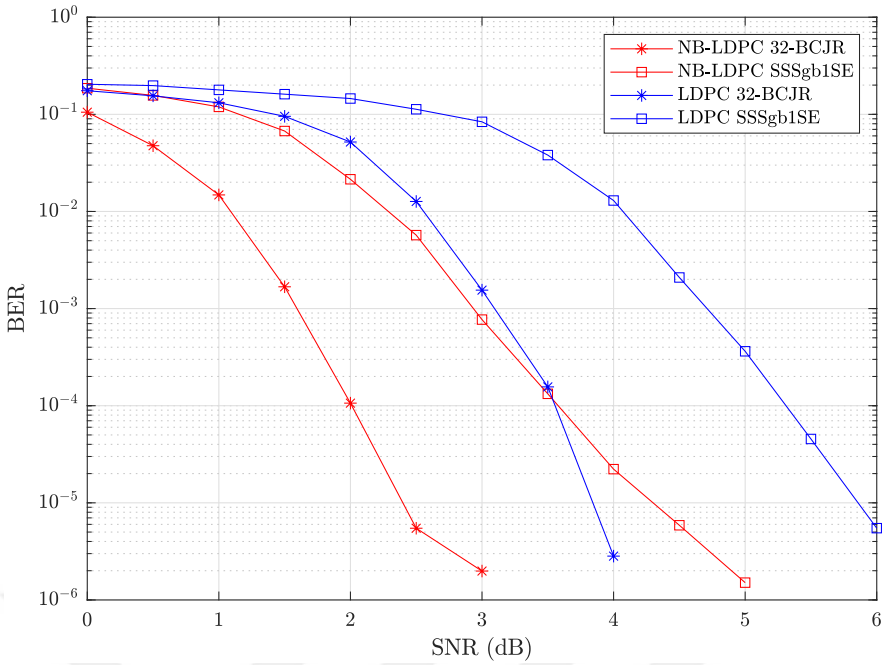

Figure 2.9 BER performance at $\tau = 0.8$, LDPC(512,256), NB-LDPC(504,252)

Continuing, the subsequent Figures, namely 2.7, 2.8, and 2.9, visually illustrate the bit error rate (BER) performances of the M-BCJR and SSSgb$K$SE detection algorithms applied to LDPC and NB-LDPC channel codes in the context of $\tau = 0.8$. Notably, in Figure 2.7, the NB-LDPC(120,60) coupled with the SSSgb$K$SE exhibits superior performance compared to LDPC(128,64) with M-BCJR algorithm, maintaining an advantage up to a signal-to-noise ratio (SNR) of 3.8 dB.

The latter demonstrates improved performance, showcasing a marginal gap of only 0.3 dB at a bit error rate (BER) of 10^{-4}. Across varying codeword lengths, an interesting trend emerges: as the codeword length increases, the convergence point between NB-LDPC(N,K) with SSSgb$K$SE and LDPC(N,K) with M-BCJR becomes increasingly closer to the targeted BER of 10^{-4}. The results are promising, even though NB-LDPC(N,K) with SSSgb$K$SE demonstrates lower performance compared to LDPC(N,K) with M-BCJR.

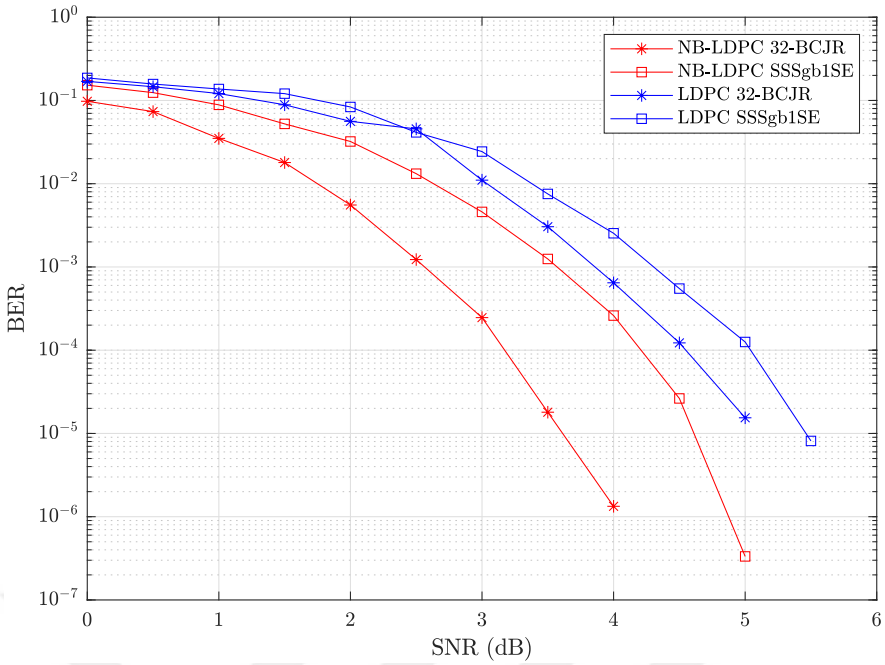

Figure 2.10 BER performance at $\tau = 0.9$, LDPC(128,64), NB-LDPC(120,60)

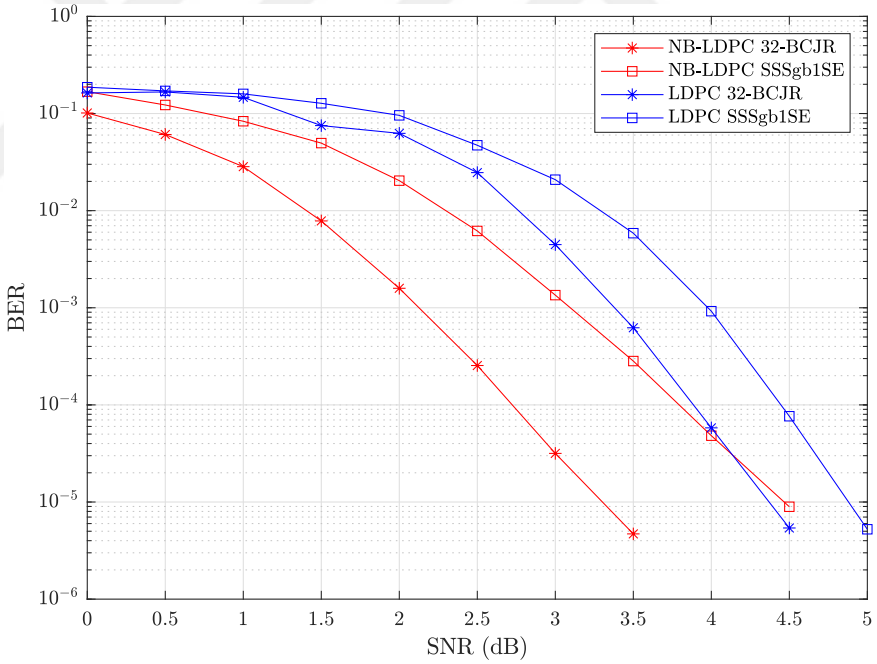

Figure 2.11 BER performance at $\tau = 0.9$, LDPC(256,64), NB-LDPC(264,132)

Shifting our focus to the case of $\tau = 0.9$ and referring to Figures 2.10, 2.11, and 2.12, a clear trend emerges. In this scenario, NB-LDPC with SSSgb$K$SE detection consistently outperforms LDPC with M-BCJR detection. Notably, at a bit error rate (BER) of 10^{-4}, NB-LDPC with SSSgb$K$SE demonstrates performance enhancements of 0.35 dB, 0.1

dB, and 0.55 dB for three distinct codeword lengths when compared to LDPC with M-BCJR detection.

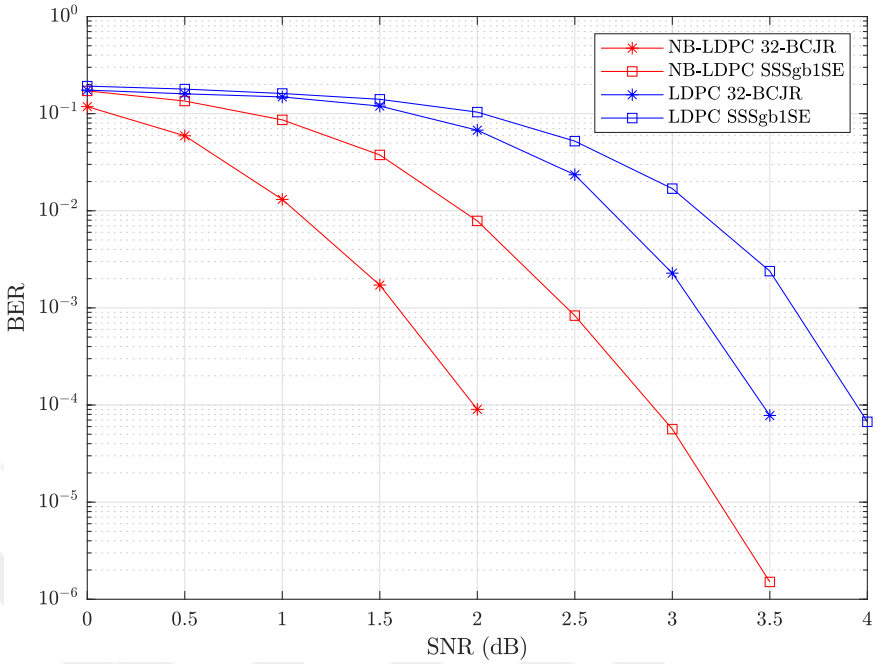

Figure 2.12 BER performance at $\tau = 0.9$, LDPC(512,256), NB-LDPC(504,252)

CHAPTER 3

COORDINATE INTERLEAVED FTN SIGNALING

In this chapter, we introduce the concept of coordinate interleaved FTN signaling (CI-FTN) [28], accompanied by a straightforward and low-complexity FTN detector tailored for CI-FTN signaling.

3.1 Literature review

In the literature, different low-complexity methods are adopted on the transmitter or receiver sides to handle the ISI of FTN signaling. At the receiver, the received symbols corrupted by the ISI are recovered with detection methods such as truncated Viterbi and M-BCJR algorithms [11], frequency-domain equalization (FDE)-assisted FTN receiver architecture [29], low-complexity symbol-by-symbol based detector [17], reduced-complexity M-BCJR algorithm based on the Ungerboeck observation model [30], and sum-product detector with deep learning approach [31]. At the transmitter side, the Tomlinson-Harashima precoded FTN signaling system with a detector using an iterative successive interference cancelation (SIC) scheme in [32]. An FTN signaling with linear precoding that combines cyclic prefix, suffix, and discrete Fourier transform with existing linear precoding algorithms is introduced in [33]. The precoding method has lower complexity than the non-linear counterparts such as THP; however, adding a prefix and suffix causes a reduction in the spectral efficiency. Also, Cholesky-decomposition aided precoding scheme with lower complexity and decoding matrix storage space consumption is applied for FTN signaling in [34].

The techniques in the literature consider ISI as an undesirable effect and try to minimize the effect of ISI to achieve better performance. In an FTN system, the effect of the ISI on a given data symbol can be either constructive or destructive. Figure 3.1 examplifies constructive and destructive interference effects for a simple case of the transmission of two consecutive binary phase shift keying (BPSK) symbols of $(+1,+1)$ and $(+1,-1)$, respectively. In other words, it shows that if we sample the first

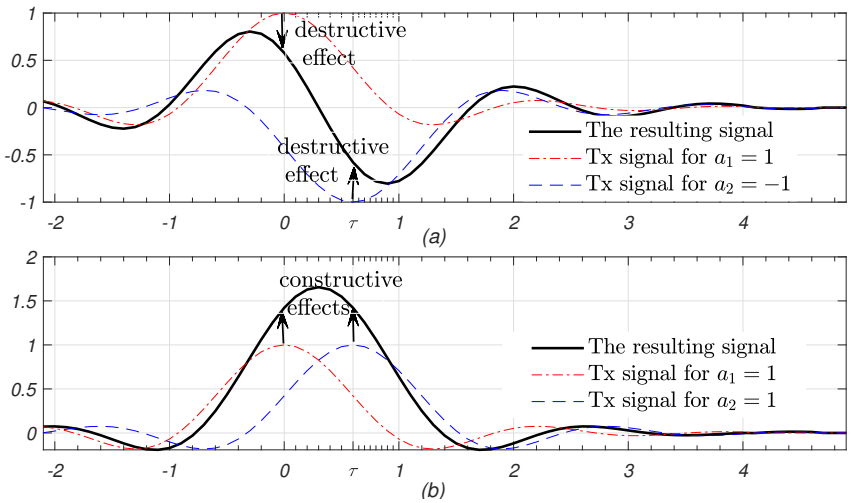

Figure 3.1 The destructive *(a)* and constructive *(b)* ISI effects for $\tau = 0.6$

signal at $t = 0$ (red line) or the second signal at $t = \tau T$ (the blue one) at the receiver, the neighboring signal may change the amplitude of the sampled symbol that will decrease or increase as in (a) and (b), respectively, depending on the sign. Therefore, at the transmitter, if more constructive interference can be generated by ordering the same signal symbols consecutively, the generated constructive effect might help to boost the performance of the FTN signaling. In this work, we introduce a simple FTN transmission method, which benefits from the ISI present on FTN signaling to improve the system performance with a negligible complexity increase. Inspired by the idea of coordinate interleaving proposed in [35], we first rotate the BPSK symbols counter-clockwise and then interleave the real and imaginary components of the rotated symbols such that the consecutive symbols possess the same signs. Having signal pairs with the same polarity guarantees constructive interference between the adjacent FTN symbols, which contributes to the symbol power by reducing destructive ISI from the adjacent symbol, and hence improves the performance. Moreover, proposed coordinate interleaved FTN (CI-FTN) signaling also reduces the total destructive ISI within a single block of symbols and improves the overall detection performance. Please note that the BPSK CI-FTN signaling can be viewed as a combination of the QPSK FTN signaling and repetition coding, where the symbols of the same sign are back to back. In this way, consecutive symbols with the same sign allow ISI reduction and a very low complexity detector design in the FTN signaling environment.

The chapter's organization is as follows: In Section 3.2, we provide an explanation of the CI-FTN signaling system model. Moving on to Section 3.3, we delve into the topic of ISI within the CI-FTN signaling system. Section 3.4 elaborates on the proposed detector and offers a complexity comparison against the BCJR algorithm and other detectors from the literature. Finally, Section 3.5 presents the simulation results.

3.2 System Model

The system model of the proposed CI-FTN signaling is shown in Figure 3.2. At the transmitter side, K-bit streams are encoded to N-length codewords in channel encoder with the coderate K/N and then the encoded bits are mapped to BPSK data symbols $a_n, n = 1, ..., N$, each of energy E_b, that are *counter-clockwise* rotated by an angle $\theta = \pi/4$ as can be seen from rotated modulation block in Figure 3.2. The counter-clockwise rotated BPSK symbols $s_n, n = 1, ..., N$, are given as

$$s_n = a_n \exp(j\theta) = s_{\mathrm{I},n} + j s_{\mathrm{Q},n}, \quad n = 1, ..., N, \tag{3.1}$$

where $s_{\mathrm{I},n}$ and $s_{\mathrm{Q},n}$ represent the I and Q components of the rotated nth BPSK data symbol, respectively, and $j = \sqrt{-1}$. After rotation, we perform the CI on every two consecutive symbols s_n and s_{n+1}, $n = 1, ..., N$, to produce two new symbols x_n and x_{n+1} that consist of the in-phase and quadrature components of s_n and s_{n+1}, respectively.

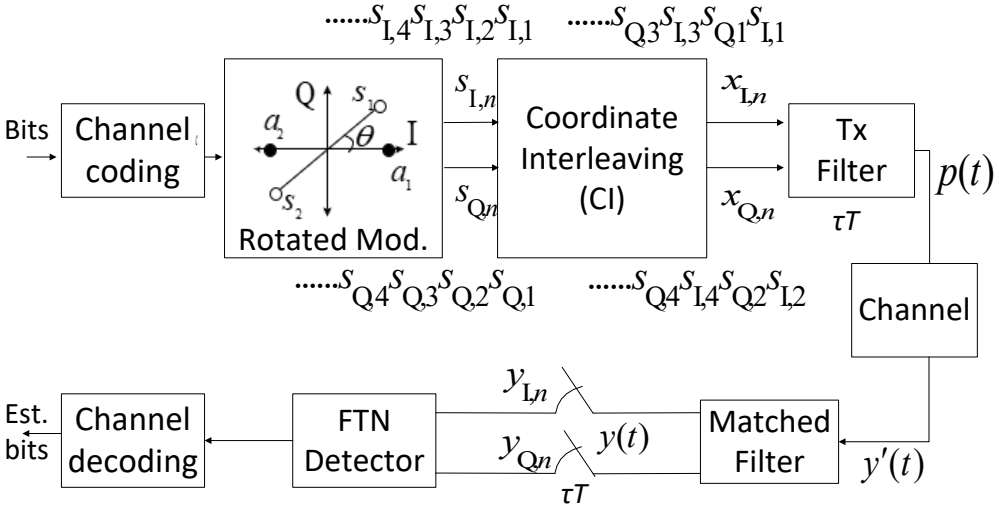

Figure 3.2 CI-FTN signaling system model.

The CI can be formally expressed as

$$x_n = f(s_n) = \begin{cases} s_{\mathrm{I},n} + j s_{\mathrm{I},n+1}, & \text{if } n \text{ is odd} \\ s_{\mathrm{Q},n-1} + j s_{\mathrm{Q},n}, & \text{if } n \text{ is even} \end{cases}, \tag{3.2}$$

where x_n is the nth interleaved symbol, and $f(\cdot)$ is a function representing the interleaving operation. The CI operation described earlier ensures that we transmit the I and Q components of the odd numbered counter-clockwise rotated BPSK symbol using the in-phase channel, while sending the I and the Q components of the even numbered counter-clockwise rotated BPSK symbols on the quadrature channel. Hence, it is important that the rotation is done counter-clockwise to guarantee that the I and Q components of any BPSK data symbol will have the same sign. In other words, if the inputs to the CI on the in-phase and quadrature channels are $\{s_{\mathrm{I},1}, s_{\mathrm{I},2}, ..., s_{\mathrm{I},N}\}$ and $\{s_{\mathrm{Q},1}, s_{\mathrm{Q},2}, ..., s_{\mathrm{Q},N}\}$, respectively, then the outputs of the CI on the in-phase and quadrature channels are $\{s_{\mathrm{I},1}, s_{\mathrm{Q},1}, ..., s_{\mathrm{I},N-1}, s_{\mathrm{Q},N-1}\}$ and $\{s_{\mathrm{I},2}, s_{\mathrm{Q},2}, ..., s_{\mathrm{I},N}, s_{\mathrm{Q},N}\}$, respectively. Please note that the CI operation does not increase the number of time slots required to transmit the N BPSK symbols, and it uses two dimensions for the BPSK modulation; hence, the spectral efficiency (SE) of the BPSK CI-FTN signaling is compared with QPSK Nyquist signaling.

Following the CI block, the interleaved symbols, x_n, $n = 1, .., N$ is transmitted through a unit energy root raised cosine (rRC) transmit filter every τT, where τ is the acceleration parameter and T is the symbol duration. The transmit signal is expressed as

$$p(t) = \zeta \sum_{n=1}^{N} x_n h(t - n\tau T), \tag{3.3}$$

where ζ is a normalization factor to ensure equal transmit energy of the CI-FTN signaling when compared to conventional FTN signaling. In this work, we consider an additive white Gaussian noise (AWGN) channel; hence, the received signal $y'(t)$ can be given as

$$y'(t) = p(t) + w(t), \tag{3.4}$$

where $w(t)$ is a zero mean noise with a covariance of $\sigma^2 \boldsymbol{I}$, where $\boldsymbol{I}$ is identity matrix.

At the receiver side, the received signal is passed through a filter matched to the rRC transmit filter. The matched filter output is written as

$$y(t) = \zeta \sum_{n=1}^{N} x_n g(t - n\tau T) + q(t), \tag{3.5}$$

where $g(t) = \int h(x')h(x'-t)dx'$, $q(t) = \int w(x')h(x'-t)dx'$. Since we transmit the symbols at a rate of $1/(\tau T)$, the output of the matched filter is sampled at the same rate. Next, the sampled signal is processed using the FTN detector block, and its soft output is input into the channel decoder. Finally, the decoder decodes them and then outputs the bit streams. Now we formulate the optimal detection rule for the proposed CI-FTN signaling. The sampled signal in Equation **3.5** can be expressed in a vector form as

$$\mathbf{y} = \zeta \mathbf{G}\mathbf{x} + \mathbf{q}, \tag{3.6}$$

where $\mathbf{G}$ is the $N \times N$ ISI matrix, and $\mathbf{x} = f(\mathbf{s}) = f(\mathbf{a}\exp(j\theta))$ is the vector of the interleaved symbols, and $\mathbf{q}$ is an $N \times 1$ zero-mean sampled noise vector with covariance of $\sigma^2\mathbf{G}$. Assuming that $\mathbf{G}$ is invertible, Equation **3.6** can be also written as

$$\begin{aligned} \mathbf{z} &= \frac{1}{\zeta}\mathbf{G}^{-1}\mathbf{y} \\ &= \mathbf{x} + \frac{1}{\zeta}\mathbf{G}^{-1}\mathbf{q}, \end{aligned} \tag{3.7}$$

where the left hand side $\frac{1}{\zeta}\ \mathbf{G}^{-1}\mathbf{y}$ can be thought of as a Gaussian random variable $\mathbf{z}$ with a covariance matrix given by

$$\Delta = \sigma^2 \frac{1}{\zeta^2}\mathbf{G}^{-1}, \tag{3.8}$$

and a mean vector $\mathbf{x}$. Hence, probability density function (pdf) of $\mathbf{z}$ is written as

$$P(\mathbf{z}|\mathbf{x}) = \frac{1}{\sqrt{(2\pi)^N|\Delta|}}\exp(-\frac{1}{2}(\mathbf{z}-\mathbf{x})^{\mathbf{T}}\Delta^{-1}(\mathbf{z}-\mathbf{x})), \tag{3.9}$$

where $|\Delta|$ is the determinant of Δ. Finding a sequence $\hat{\mathbf{x}}$ to maximize Equation **3.9** is known as the maximum likelihood sequence estimation (MLSE). Since maximizing Equation **3.9** is equivalent to minimizing the exponent part in Equation **3.9**, the MLSE

problem for the CI-FTN signaling can be expressed as

$$\mathcal{OP}_{\text{MLSE}} : \hat{\mathbf{a}} = \underset{\mathbf{a}\in D}{\arg\min}\left(\left(\mathbf{z} - f(\mathbf{a}\exp(j\theta))\right)^{\mathrm{T}}\Delta^{-1}\left(\mathbf{z} - f(\mathbf{a}\exp(j\theta))\right)\right). \quad (\mathbf{3.10})$$

Finding the optimal solution to the MLSE in Equation **3.10** is of high-complexity. In Section IV, we discuss a low-complexity detection technique for the CI-FTN signaling.

3.3 ISI on the CI-FTN singaling

This section examines the effect of coordinate interleaving on ISI that affects the symbol. It shows how the CI-FTN signaling reduces destructive ISI in a single symbol block at different τ values compared to the traditional FTN signaling.

As explained in the previous section, after the CI operation at the transmitter the odd-numbered and even-numbered counter-clockwise rotated BPSK symbol components exist on the in-phase and quadrature channels, respectively. This ensures that every two interleaved consecutive symbol components will have the same sign and thus decreasing the power loss at the receiver side compared to conventional FTN signaling as the CI-FTN signaling reduces destructive interference, which may cause the detector to make a wrong decision.

In order to better understand the advantages of the proposed CI-FTN method, we will give a numerical example in the absence of channel noise. Let us consider transmitting the following sequence of 6 BPSK symbols [1 −1 1 −1 1 1] and examine the ISI effects on the third symbol for the case of $\tau = 0.6$. In conventional FTN signaling, the real part of the sequence after matched filter is [0.5250 0.1154 −0.3340 −0.0988 1.0166 1.4706]. In this case, the third symbol gets a total ISI of −1.3340 and the resulting symbol value becomes −0.3340, which has a flipped sign compared to the transmitted symbol sign. On the other hand, when the CI-FTN method is used for the same sequence, we transmit [0.5794 - 0.5794i 0.5794 - 0.5794i 0.5794 - 0.5794i 0.5794 - 0.5794i 0.5794 + 0.5794i 0.5794 + 0.5794i]. Consequently, the I and Q components of the 3 rd symbol, namely $x_{I,3}$ and $x_{I,4}$ according to Figure 3.2 are now adjacent and constructive to each other, which helps to make a correct detection.

Table 3.1 ISI values at different values of τ.

	Conventional FTN signaling		CI-FTN signaling	
τ	Symbol	ISI values	ISI values	I or Q
0.9	1	0.5388	0.0464	0.5794
0.8	1	0.9727	0.0649	0.5794
0.7	1	1.2913	0.1552	0.5794
0.6	1	1.6580	0.2349	0.5794
0.5	1	1.8547	0.3718	0.5794
0.4	1	2.8911	0.7278	0.5794

Thus, ordering the same sign components consecutively in the CI-FTN signaling technique reduces the individual ISI on each symbol component, which leads to a considerable reduction in the overall interference within a symbol block. Based on the worst-case sequence, Table 3.1 shows ISI values experienced by a symbol within a sequence of $2L$ symbols in the conventional FTN and CI-FTN signaling for different values of τ, where L is the length of the single-sided ISI vector. For example, for $\tau = 0.6$, while a symbol can experience ISI up to 165% of the magnitude of the symbol in conventional FTN signaling, a symbol component (I or Q) is exposed to ISI up to 47% of the magnitude of the component in the CI-FTN signaling at $\tau = 0.6$. This significant ISI reduction in the CI-FTN signaling is achieved by exposing the consecutive components with the same sign.

3.4 A Simple Detector for the CI-FTN Technique

In this section, we introduce a low-complexity detector for the proposed CI-FTN signaling, which strikes a balance between computational complexity and performance. The proposed low-complexity detector exploits the fact that the I and Q components of each interleaved pair belong to the same BPSK data symbol, and hence, should have the same sign. As discussed earlier, the I and Q components of the rotated BPSK symbols s_k and s_{k+1} are interleaved with each other to produce two interleaved symbols x_k and x_{k+1} as described in Equation **3.2**.

After the matched filter and sampler, the I components of the first two received samples

$y_{\mathrm{I},k}$ and $y_{\mathrm{I},k+1}$ can be expressed as

$$\begin{aligned} y_{\mathrm{I},k} = & \underbrace{\zeta G_{kk} \overbrace{x_{\mathrm{I},k}}^{s_{\mathrm{I},k}}}_{\text{I component of the } k\text{th symbol}} + \underbrace{\zeta G_{k(k+1)} \overbrace{x_{\mathrm{I},k+1}}^{s_{\mathrm{Q},k}}}_{\text{constructive ISI}} \\ & + \underbrace{\zeta \sum_{i=1}^{L-1} x_{\mathrm{I},k-i} G_{k(k-i)}}_{\text{ISI from previous components}} + \underbrace{\zeta \sum_{i=2}^{L} x_{\mathrm{I},k+i} G_{k(k+i)}}_{\text{ISI from upcoming components}} \\ & + q_{\mathrm{I},k}. \end{aligned} \tag{3.11}$$

$$\begin{aligned} y_{\mathrm{I},k+1} = & \underbrace{\zeta G_{(k+1)(k+1)} \overbrace{x_{\mathrm{I},k+1}}^{s_{\mathrm{Q},k}}}_{\text{Q component of the } k\text{th symbol}} + \underbrace{\zeta G_{(k+1)k} \overbrace{x_{\mathrm{I},k}}^{s_{\mathrm{I},k}}}_{\text{constructive ISI}} \\ & + \underbrace{\zeta \sum_{i=2}^{L} x_{\mathrm{I},k+1-i} G_{(k+1)(k+1-i)}}_{\text{ISI from previous components}} \\ & + \underbrace{\zeta \sum_{i=1}^{L-1} x_{\mathrm{I},k+1+i} G_{(k+1)(k+1+i)}}_{\text{ISI from upcoming components}} + q_{\mathrm{I},k+1}, \end{aligned} \tag{3.12}$$

Similarly, the received samples on the Q channel can also be written for the $y_{\mathrm{Q},k}$ and $y_{\mathrm{Q},k+1}$ signals.

As can be seen from Equation **3.11** and Equation **3.12**, the component interleaving guarantees that dominant ISI term that comes from the adjacent symbol within a pair of symbols is constructive. To estimate the transmitted symbol s_k, the proposed detector must jointly consider $y_{\mathrm{I},k}$ and $y_{\mathrm{I},k+1}$ as both samples correspond to the I and Q components of the same data symbol s_k. Likewise, the samples $y_{\mathrm{Q},k}$ and $y_{\mathrm{Q},k+1}$ are processed jointly to determine the transmitted symbol s_{k+1}. As the components of a symbol are exposed to different levels of interference, there exists a diversity benefit at the receiver. To utilize this diversity, the simplest approach would be to add $y_{\mathrm{I},k}$ and $y_{\mathrm{I},k+1}$ before starting the detection process.

In Equation **3.13**, it is shown that when added together, all the terms with the same sign as s_k are combined to obtain a more reliable sample for the estimation of s_k. The proposed detector for the CI-FTN technique is formally described in Algorithm 1,

where the detection process is started after receiving at least L samples on each of the I and Q channels, where $L << N$ is the one sided ISI length.

$$
\begin{aligned}
y_{\mathrm{I},k} + y_{\mathrm{I},k+1} = \quad & \underbrace{\zeta G_{kk} \overbrace{x_{\mathrm{I},k}}^{s_{\mathrm{I},k}} + \zeta G_{(k+1)(k+1)} \overbrace{x_{\mathrm{I},k+1}}^{s_{\mathrm{Q},k}}}_{\text{sum of the terms with the same sign as } k\text{th symbol}} \\
+ \quad & \underbrace{\zeta G_{k(k+1)} \overbrace{x_{\mathrm{I},k+1}}^{s_{\mathrm{Q},k}} + \zeta G_{(k+1)k} \overbrace{x_{\mathrm{I},k}}^{s_{\mathrm{I},k}}}_{\text{sum of the terms with the same sign as } k\text{th symbol}} \\
+ \quad & \underbrace{\zeta \sum_{i=1}^{L-1} x_{\mathrm{I},k-i} G_{k(k-i)}}_{\mathrm{ISI}_k \text{ sum of ISI from previous components for } k\text{th sample}} \\
+ \quad & \underbrace{\zeta \sum_{i=2}^{L} x_{\mathrm{I},k+i} G_{k(k+i)}}_{\mathrm{ISI}_k \text{ sum of ISI from upcoming components for } k\text{th sample}} \\
+ \quad & \underbrace{q_{\mathrm{I},k}}_{\text{noise sample for } k\text{th sample}} \\
+ \quad & \underbrace{\zeta \sum_{i=2}^{L} x_{\mathrm{I},k+1-i} G_{(k+1)(k+1-i)}}_{\mathrm{ISI}_{k+1} \text{ sum of ISI from previous components for } (k+1)\text{th sample}} \\
+ \quad & \underbrace{\zeta \sum_{i=1}^{L-1} x_{\mathrm{I},k+1+i} G_{(k+1)(k+1+i)}}_{\mathrm{ISI}_{k+1} \text{ sum of ISI from upcoming components for } (k+1)\text{th sample}} \\
+ \quad & \underbrace{q_{\mathrm{I},k+1}}_{\text{noise sample for } (k+1)\text{th sample}} .
\end{aligned}
\tag{3.13}
$$

where $G_{\mu\nu}$ is an element of the ISI matrix $\mathbf{G}$ which represents the ISI effect of νth symbol on the μth symbol. Please note that waiting for L samples to start the detection process does not have any negative effect on latency, since system latency is usually determined by the block length of channel codes, which is generally much larger than L. In Algorithm 1, to detect the symbol a_k, first the two components of a symbol, $y_{\mathrm{I},k}$ and $y_{\mathrm{I},k+1}$, which are in the same pair and have the same sign, are summed together. Then, L received samples on both sides of $s_{\mathrm{I},k}$ and $s_{\mathrm{Q},k}$, and the ISI on them are estimated. Note that the ISI consists of ISI_{k+1} and ISI_k which represent the total ISI amount from the previous and upcoming components outside of $x_{\mathrm{I},k}$ and $x_{\mathrm{I},k+1}$ component pair on kth and $(k+1)$th components, respectively. These ISI values are calculated using the

Algorithm 1 Proposed CI-FTN detector

Inputs: $\boldsymbol{y}, \boldsymbol{G}, L, N, \theta, \zeta$
Outputs: $\hat{\boldsymbol{a}}$
Initialization:
$k \leftarrow 1$
$n \leftarrow 1$
for $k < N$ **do**
  $\text{sumIQ}_\text{k} = y_{\text{I},k} + y_{\text{I},k+1}$
  for $k - L \leq n \leq k + L$ **do**
    Calculate ISI_k, ISI_{k+1}
    $n \leftarrow n + 1$
  end for
  $\hat{a}_k \leftarrow \text{quantize}(\text{sumIQ}_\text{k} - \text{ISI}_{k+1} - \text{ISI}_k)$
  $k \leftarrow k + 2$
end for
return $\hat{\boldsymbol{a}}$

quantized samples for the ISI from the upcoming samples, and the estimated symbols $\hat{a}_k$ for the ISI from the previous samples. Removing the ISI due to the previous and upcoming samples, which is seen from Equation **3.11** and Equation **3.12** clearly leaves only the constructive ISI effects at $n = k + 1$ and $n = k$ on the symbol components.

The kth symbol on the I path and $(k+1)$th symbol on are estimated as in Equation **3.14** and Equation **3.15**, respectively.

$$\begin{aligned}\hat{a}_k = \text{quantize}\Big\{ y_{\text{I},k} + y_{\text{I},k+1} - \underbrace{\zeta \sqrt{\frac{1}{2}} \sum_{i=1}^{L-1} \hat{a}_{k-i} G_{k(k-i)}}_{\text{ISI from prev. sym. for } x_{\text{I},k} \text{ sample}} \\ - \underbrace{\zeta \sqrt{\frac{1}{2}} \sum_{i=2}^{L} \text{quantize}\{y_{\text{I},k+i}\} G_{k(k+i)}}_{\text{ISI from upcoming symbols for } x_{\text{I},k} \text{ component}} \\ \underbrace{- \zeta \sqrt{\frac{1}{2}} \sum_{i=1}^{L-1} \text{quantize}\{y_{\text{I},k+1+i}\} G_{(k+1)(k+1+i)}}_{\text{ISI from upcoming symbols for } x_{\text{I},k+1} \text{ component}} \\ - \underbrace{\zeta \sqrt{\frac{1}{2}} \sum_{i=2}^{L} \hat{a}_{k+1-i} G_{(k+1)(k+1-i)}}_{\text{ISI from previous symbols for } x_{\text{I},k+1} \text{ component}} \Big\},\end{aligned} \tag{3.14}$$

$$\begin{aligned}\hat{a}_{k+1} = \text{quantize}\Big\{ & y_{\text{Q},k} + y_{\text{Q},k+1} - \underbrace{\sqrt{\frac{E_s}{2}} \sum_{i=1}^{L-1} \hat{a}_{k-i} G_{k(k-i)}}_{\text{ISI from prev. sym. for } x_{\text{Q},k} \text{ comp.}} \\ & - \underbrace{\sqrt{\frac{E_s}{2}} \sum_{i=2}^{L} \text{quantize}\{y_{\text{Q},k+i}\} G_{k(k+i)}}_{\text{ISI from upcoming symbols for } x_{\text{Q},k} \text{ component}} \\ & - \underbrace{\sqrt{\frac{E_s}{2}} \sum_{i=1}^{L} \text{quantize}\{y_{\text{Q},k+1+i}\} G_{(k+1)(k+1+i)}}_{\text{ISI from upcoming symbols for } x_{\text{Q},k+1} \text{ component}} \\ & - \underbrace{\sqrt{\frac{E_s}{2}} \sum_{i=2}^{L} \hat{a}_{k+1-i} G_{(k+1)(k+1-i)}}_{\text{ISI from previous symbols for } x_{\text{Q},k+1} \text{ component}} \Big\},\end{aligned} \tag{3.15}$$

where quantize$\{\gamma\}$ rounds γ to the nearest unrotated BPSK symbol.

When it comes to the complexity of the proposed detector, as seen from Table 3.2, the proposed detector has the complexity of $O(NL)$ while the one of the BCJR detector [11] is $O(2^L N)$, meaning that its complexity increases exponentially as L increases. The work in [29] has similar complexity to the proposed detector, but requires waiting for all the N samples in the sequence for detection.

Table 3.2 Computational complexity.

Algorithm	Complexity
The proposed detector	$O(NL)$
MMSE FDE [29]	$O(NlogN)$
BCJR [11]	$O(2^L N)$

3.5 Simulation Results

In this section, we evaluate the performance of the proposed CI-FTN signaling using the proposed low-complexity detector and compare with different FTN detectors. The roll-off factor of the root raised cosine is set to $\alpha = 0.3$. We also show the LDPC coded performance of the detector against Nyquist signaling, where the code rate of $\frac{1}{2}$ and the length of the codeword of $N = 672$ are used.

In Figure 3.3, the performance of the proposed detector of the CI-FTN technique is depicted for $\tau = 0.6$, 0.5, and 0.45, and is also compared to the no ISI case (i.e., $\tau = 1$) for uncoded and channel coded scenarios. Since CI-FTN signaling with BPSK modulation uses I and Q components, its SE is compared to that in Nyquist signaling with QPSK modulation. At BER of 10^{-5}, the proposed detector of CI-FTN signaling with BPSK modulation follows the performance of Nyquist signaling with QPSK modulation for $\tau = 0.5$, with the same SE at the same bandwidth and energy despite ISI. At $\tau = 0.45$, the detector achieves $\frac{1.71-1.54}{1.71} = 10\%$ more spectral efficiency and gets close about 0.6 dB to the no ISI case ($\tau = 1$) at the cost of low complexity, compared to the Nyquist signaling with QPSK modulation. Again at BER of 10^{-5}, in the channel coded performance that the detector at $\tau = 0.45$ is compared with no ISI, there is about 0.6 dB between them. It shows that channel coding provides a gain similar to Nyquist signaling for CI-FTN signaling.

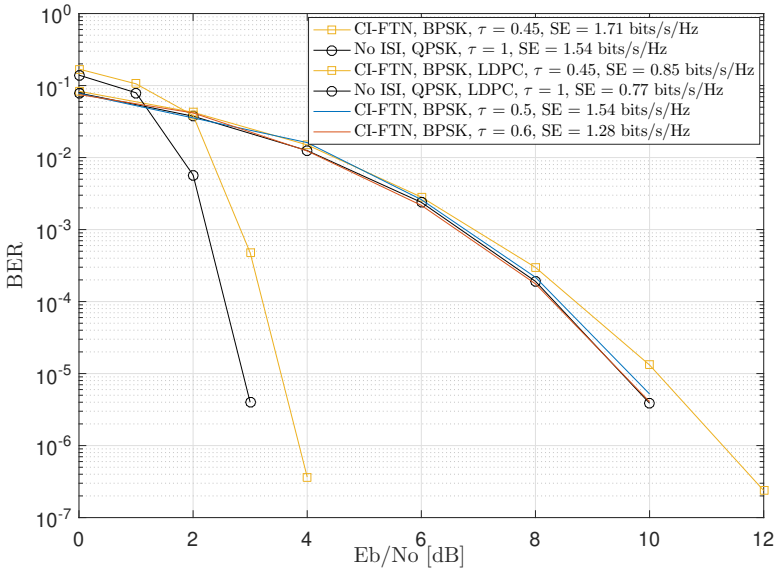

Figure 3.3 BER performance of the proposed detector, $\alpha = 0.3$.

In Figure 3.4, the performance of the low-complexity detector of CI-FTN signaling is compared to the MMSE-FDE in [29], SVD precoding in [36], and the M-BCJR in [11] with QPSK modulation after setting τ to the values that result in the same SE of 1.71 bits/s/Hz for each detector. At the BER of 10^{-4}, the M-BCJR has the same performance as at $\tau = 1$, but with more complexity. The proposed low-complexity detector gets approximately 0.3 dB closer to the no ISI case or the M-BCJR compared

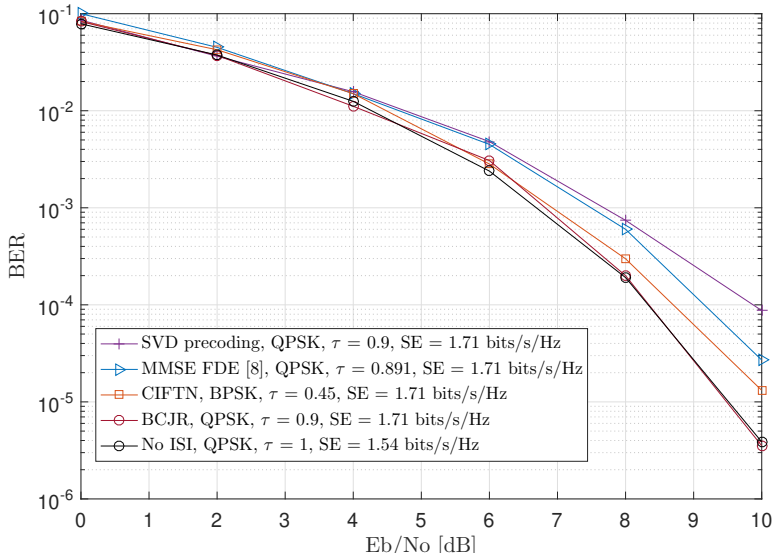

Figure 3.4 Performance comparison of the proposed detector, $\alpha = 0.3$.

to the MMSE-FDE with similar complexity to the detector, while the SVD precoding method is about 1.7 dB away from $\tau = 1$.

CHAPTER 4

LUT AIDED SOFT-OUTPUT SDR BASED DETECTOR

In this chapter, we introduce a soft-output semidefinite relaxation-based FTN signaling detector (soSDR) [37]. The modulation constellation is represented using a polynomial equation, which offers extensibility to higher modulation schemes. Log-likelihood values (LLRs) are computed through lookup tables (LUTs) based on the detector's output. We conduct a performance comparison between the soft-output soSDR and the optimal FTN signaling detector, BCJR.

4.1 Review of Related Work

With the escalating demands for higher data rates and finite spectrum resources, there is an imperative to develop bandwidth-efficient transmission techniques. Faster-than-Nyquist (FTN) signaling emerges as a potent solution in this space, using non-orthogonal pulses in the time domain to transmit more data within the same bandwidth and signal-to-noise ratio (SNR) [38]. Recent attention from both industry and academia has revived interest in FTN signaling, spotlighting its potential in various applications such as point-to-point microwave backhaul links, optical long-haul links, digital video broadcasting, satellite communications, and next-generation cellular networks with expansive antenna arrays at base stations [39]. While FTN signaling enhances spectral efficiency (SE), it introduces controlled inter-symbol interference (ISI) between neighboring pulses at the receiver. Addressing this ISI necessitates advanced signal processing techniques, which in turn add to the detection complexity. Existing reduced-complexity FTN detectors, as detailed in [15, 29, 40], offer hard output decisions for the transmitted data symbols. However, such detectors may not be fully compatible with coded communication systems. A significant advancement towards the practical deployment of FTN signaling is the development of FTN detectors that produce soft output decisions. But generating soft outputs introduces its own set of challenges, especially in crafting LLR

values for channel decoders in coded setups. The precise LLR calculation for a single bit in an N-bit sequence involves processing 2^N hard-output sequences—a daunting computational task. While the maximum a posterior probability (MAP) demapper has a complexity of $O(2^s)$, yielding the most reliable log-likelihood ratios, research such as [41] and [42] propose methods for low-complexity LLR computation. These methodologies effectively reduce the computational load from $O(2^s)$ to $O(s)$, where s denotes the number of bits per symbol.

This chapter introduces the soSDR detector tailored for coded FTN systems. SDR-based FTN detectors, as highlighted in [15] and [12], are commendable due to their good performance combined with polynomial time complexity. Our proposed soft-output generation method furnishes dependable log-likelihood ratio values for the channel decoder. This is achieved without inflating the complexity compared to the innate complexity of the semidefinite relaxation optimization. To validate the efficiency of our proposed method, we simulated the soSDR FTN detector within the context of polar codes for channel coding, comparing its performance against the benchmark BCJR detector. Simulations indicate that the soSDR detector generates reliable soft values, striking a good balance between bit error rate (BER) performance and detection complexity.

The structure of the chapter is as follows: Section 4.2 reviews the coded FTN signaling system model. The proposed soft-output semidefinite relaxation-based detector is elaborated in Section 4.3. Section 4.4 presents the complexity comparison of the soSDR against the BCJR, followed by simulation outcomes in Section 4.5.

4.2 System Model

Figure 4.1 depicts a block diagram of a polar coded communication system using FTN signaling. On the transmitter side, a sequence $\mathbf{k}$ comprising K information bits undergoes polarization through a polar encoder, leveraging a recursive butterfly structure. This process polarizes N channels into highly reliable and completely unreliable channels, respectively. The encoder yields N bits, allocating the K most reliable bit positions to information bits, termed as the free bits.

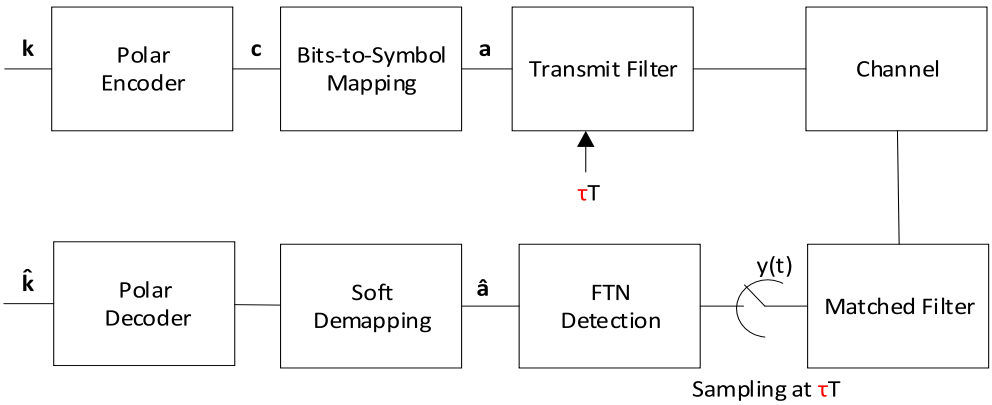

Figure 4.1 Block diagram of channel coded FTN signaling

The remaining $N-K$ positions, recognized as frozen bits, are set to a value of 0. The placement of these bits onto a vector **u** results in a polar codeword as

$$\mathbf{c} = \mathbf{uG}, \tag{4.1}$$

where **G** represents the polar code generator matrix defined as

$$\mathbf{G} = \mathbf{F}^{\otimes s}, \tag{4.2}$$

where $\otimes$ denotes the sth Kronecker power of **F** over the binary field,

$$\mathbf{F} = \begin{bmatrix} 1 & 0 \\ 1 & 1 \end{bmatrix}, \tag{4.3}$$

and s is the number of stages, expressed by

$$s = \log_2 N. \tag{4.4}$$

Each bit in the codeword **c** undergoes 4-PAM mapping, followed by shaping via a unit energy pulse $z(t)$. Symbols are transmitted every τT, where $0 < \tau \leq 1$ signifies the FTN signaling acceleration parameter, and T is the symbol duration. After this process, the signal travels through an additive white Gaussian noise channel (AWGN), represented as $w(t)$. At the receiver, to retrieve the transmitted symbols from the noisy signal, a

matched filter is employed. The output from this filter is

$$y(t) = \sqrt{\frac{K}{N}E_s}\sum_{n=1}^{N} a_n\gamma(t-n\tau T) + q(t), \tag{4.5}$$

where $\mathbf{a}$ is the sequence of symbols whose elements are the 4-PAM data, a_n, $n = 1, 2, ..., N-2, N-1, N$, and E_s is the energy of the data symbol, $\frac{K}{N}$ is the code rate, $\gamma(t) = \int z(x)z(x-t)dx$ and $q(t) = \int w(x)z(x-t)dx$. The signaling rate is $\frac{1}{\tau T}$. The received signal, denoted by $y(t)$, undergoes sampling every τT seconds, and the lth received sample can be described by

$$\begin{aligned} y_l &= y(l\tau T) \\ &= \sqrt{\frac{K}{N}E_s}\sum_{n=1}^{N} a_n\gamma(l\tau T - n\tau T) + q(l\tau T), \\ &= \underbrace{\sqrt{\frac{K}{N}E_s}a_l\gamma(0)}_{\text{desired symbol}} \\ &+ \underbrace{\sqrt{\frac{K}{N}E_s}\sum_{n=1,n\neq l}^{N} a_n\gamma(l\tau T - n\tau T)}_{\text{ISI}} \\ &+ \underbrace{q(l\tau T)}_{l\text{th noise sample after matched filter}}. \end{aligned} \tag{4.6}$$

From Equation **4.6**, the received signal encompasses the desired symbol, noise, and ISI. The signal can be vectorized as

$$\mathbf{y} = \sqrt{\frac{K}{N}E_s}\mathbf{a} * \gamma + \mathbf{q_c}, \tag{4.7}$$

where $\mathbf{q_c}$ is the colored noise, * is the convolution operator, and γ is the ISI vector. Subsequently, we can represent Equation **4.7** in the form

$$\mathbf{y} = \mathbf{G}\mathbf{a} + \mathbf{q_c}, \tag{4.8}$$

where $\mathbf{G}$ is the ISI matrix and $\mathbf{q_c}$ is the colored noise with probability density function of $\mathcal{N}(\mathbf{0}, \sigma^2\mathbf{G})$. A whitening matched filter is designed to whiten the noise spectrum.

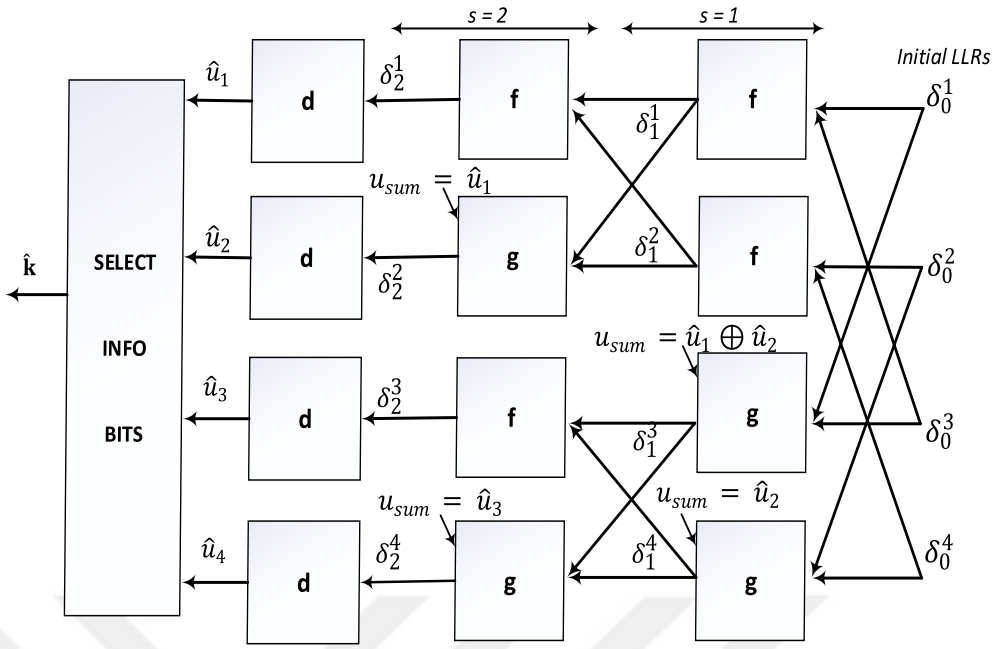

Figure 4.2 Successive cancellation decoding of polar codes for $N = 4$ bits

The received vector is then

$$\mathbf{y} = \mathbf{Va} + \mathbf{q_w}, \tag{4.9}$$

where $\mathbf{V}$ denotes the newly constructed ISI matrix based on the causal ISI vector. $\mathbf{q_w}$ represents the whitened noise, having a probability density function $\mathcal{N}(\mathbf{0}, \sigma^2\mathbf{I})$, with I being the identity matrix. This allows us to formally present the maximum likelihood sequence estimation (MLSE) problem at the receiver as

$$\underset{a}{\text{minimize}} \quad \|\mathbf{y} - \mathbf{Va}\|_2^2, \tag{4.10}$$

where a represents an $N \times 1$ symbol vector derived from the relevant alphabet constellation. To address the detection problem presented in Equation **4.10**, we propose an SDR-based FTN signaling detector. This detector efficiently produces soft outputs utilizing lookup tables (LUTs), ensuring a minimal increase in computational complexity compared to its hard-output counterpart. Soft outputs derived from solving the detection problem in Equation **4.10** serve as the initial LLR input to the polar decoder. Within this polar decoder, the successive cancellation decoding algorithm (SCD) is employed to estimate the bit sequence $\hat{\mathbf{k}}$ [43]. Figure 4.2 provides an illustration of a 4-bit SCD example, utilizing three distinct functions: f, g, and d.

Inputs δ_0^i and $\hat{u}_i$ $(i = 1,2,3,4)$ correspond to the initial LLR value and the hard decision for the ith bit, respectively. Functions f and g essentially reverse the encoder operations as detailed in Equation **4.11** to Equation **4.13**. These operations use the LLR values from the preceding stage and the partial sums of earlier decoded bits u_{sum} to determine the LLR values for the subsequent stage.

$$\delta_{j+1}^i = \begin{cases} f\left(\delta_j^i, \delta_j^{i+\frac{N}{2^{j+1}}}\right), \\ g\left(\delta_j^{i-\frac{N}{2^{j+1}}}, \delta_j^i, \hat{u}_{\text{sum}}\right), \end{cases} \tag{4.11}$$

$$f(\mu,\nu) = \text{sign}(\mu)\,\text{sign}(\nu)\min(|\mu|,|\nu|), \tag{4.12}$$

$$g(\mu,\nu,u_{\text{sum}}) = (-1)^{u_{\text{sum}}}\mu + \nu, \tag{4.13}$$

where δ_{j+1}^i is the LLR value of ith bit at $(j+1)$th stage. $\text{sign}(\cdot)$ gives the sign of $(\cdot)$ while $\min(\cdot,\cdot)$ produces the minimum. In Equation **4.13**, the partial sum of the previously decoded bit, u_{sum}, is propagated back into the LLR estimation of the next stage. The u_{sum} values of stage 1 and 2 are given as

$$u_{sum} = \begin{cases} \hat{u}_1 \oplus \hat{u}_2 \text{ , } \hat{u}_2 \text{ at } s = 1, \\ \hat{u}_1 \text{ , } \hat{u}_3 \text{ at } s = 2, \end{cases} \tag{4.14}$$

where $\oplus$ is a logical xor operation. In this way, all bits are decoded at $s = \log_2 N$ stages successively. Finally, the hard decisions $\hat{u}_1^N$, $i = 1,2,...,N-2,N-1,N$ based on the updated LLR values δ_{j+1}^i, $i = 1,2,...,N-2,N$; $j = 0,1,...,s-2,s-1$ are calculated as in Equation **4.15** and then the information sequence $\hat{\mathbf{k}}$ (free bits) is selected from $\hat{u}_1^N$ according to their indices. In the process of decoding, each bit is successively decoded over s stages. Finally, based on the updated LLR values, the hard decisions are derived as demonstrated in Equation **4.15**. Subsequently, the information sequence $\hat{\mathbf{k}}$ is extracted from $\hat{u}_1^N$ based on their indices.

$$\hat{u}_i = \begin{cases} 1, \delta_s^i \geq 0 \\ 0, \delta_s^i < 0. \end{cases} \tag{4.15}$$

4.3 Low-Complexity Soft-Output SDR Based FTN Detector

In this section, we present a soft-output SDR-based FTN detector, which has a similar polynomial detection complexity order to the hard-output SDR detector. The objective function described in Equation **4.10** can be reformulated as

$$\begin{aligned} \|\mathbf{y}-\mathbf{V}\mathbf{a}\|^2 &= (\mathbf{y}-\mathbf{V}\mathbf{a})^{\mathbf{T}}(\mathbf{y}-\mathbf{V}\mathbf{a}), \\ &= \mathbf{y}^{\mathbf{T}}\mathbf{y}-\mathbf{y}^{\mathbf{T}}\mathbf{V}\mathbf{a}-\mathbf{a}^{\mathbf{T}}\mathbf{V}^{\mathbf{T}}\mathbf{y}+\mathbf{a}^{\mathbf{T}}\mathbf{V}^{\mathbf{T}}\mathbf{V}\mathbf{a}, \\ &= \|\mathbf{y}\|^2-2\mathbf{a}^{\mathbf{T}}\mathbf{V}^{\mathbf{T}}\mathbf{y}+\mathbf{tr}\{\mathbf{V}^{\mathbf{T}}\mathbf{V}\mathbf{A}\}, \end{aligned} \tag{4.16}$$

where $\mathbf{A}=\mathbf{a}\mathbf{a}^{\mathbf{T}}$ is $N\times N$ symmetric positive semidefinite matrix and $\mathbf{tr}\{.\}$ is the trace operator. Since $\|\mathbf{y}\|^2$ is independent of $\mathbf{a}$, The M-PAM FTN signaling detection problem can be expressed as

$$\hat{a}=\arg\min_{\mathbf{a}\in\mathcal{M}^{N\mathrm{x}1}} \quad \mathbf{tr}\{\mathbf{V}^{\mathbf{T}}\mathbf{V}\mathbf{A}\}-2\mathbf{a}^{\mathbf{T}}\mathbf{V}^{\mathbf{T}}\mathbf{y}, \tag{4.17}$$

where $\mathcal{M}$ represents the modulation alphabets. The FTN signaling detection problem in Equation **4.17** is a nonconvex problem with rank one constraint due to $\mathbf{A}=\mathbf{a}\mathbf{a}^{\mathbf{T}}$; hence, it is hard to solve. We relax this rank one constraint, [12] adding a convex positive semidefinite constraint of $\mathbf{A}-\mathbf{a}\mathbf{a}^{\mathbf{T}}\geq 0$. Now, the general optimization form of the FTN signaling detection problem in Equation **4.17** can be written as

$$\begin{aligned} &\hat{a}=\arg\min_{\mathbf{a}\in\mathcal{M}^{N\mathrm{x}1}} \mathbf{tr}\{\mathbf{V}^{\mathbf{T}}\mathbf{V}\mathbf{A}\}-2\mathbf{a}^{\mathbf{T}}\mathbf{V}^{\mathbf{T}}\mathbf{y} \\ &\text{subject to } \textit{constraints based on the modulation schemes} \\ &\qquad \mathbf{A}-\mathbf{a}\mathbf{a}^{\mathbf{T}}\succeq\mathbf{0}. \end{aligned} \tag{4.18}$$

by denoting the constellation alphabet by polynomial constraints [44]: $(a-p_M)...(a-p_1)(a-p_2)(a+p_1)(a+p_2)...(a+p_M)$, where $p_1, p_2, ...,$ and p_M are constellation points. For the purpose of elucidation, the polynomial expression for a 4-PAM modulation becomes: $(a-3)(a-1)(a+1)(a+3)=b^2-10b+1$. Using $a^2=b$ the problem is

detailed as

$$\begin{aligned} \min_{\mathbf{X}} \quad & \mathbf{tr}\{\mathbf{\Omega X}\} \\ \text{s.t.} \quad & \text{diag}\{\mathbf{X}_{1\ldots N,1\ldots N}\} - \mathbf{X}_{N+1\ldots 2N,2N+1} = 0 \\ & \text{diag}\{\mathbf{X}_{N+1\ldots 2N,N+1\ldots 2N}\} - 10\mathbf{X}_{N+1\ldots 2N,2N+1} + 9 = 0 \\ & \mathbf{X}_{2N+1,2N+1} = 1 \end{aligned} \tag{4.19}$$

where the objective function in Equation **4.17** is written in the form of $\mathbf{tr}\{\mathbf{\Omega X}\}$ using

$$\Omega = \begin{bmatrix} \mathbf{V^T V} & \mathbf{0} & -\mathbf{V^T y} \\ \mathbf{0} & \mathbf{0} & \mathbf{0} \\ -\mathbf{y^T V} & \mathbf{0} & \mathbf{y^T y} \end{bmatrix}_{2N+1 \text{x} 2N+1}, \tag{4.20}$$

and

$$\mathbf{X} = \begin{bmatrix} \mathbf{a} & \mathbf{b} & \mathbf{1} \end{bmatrix}_{2N+1 \text{x} 1} \begin{bmatrix} \mathbf{a^T} & \mathbf{b^T} & \mathbf{1} \end{bmatrix}_{1 \text{x} 2N+1}, \tag{4.21}$$

as in [45]. In this context, the optimization focuses on the variable matrix $\mathbf{X}$, which encompasses the symbol sequence $\mathbf{a}$. It is worth noting that the size N of the polynomial constraints in the detection problem proportionally increases as the modulation level rises. This expansion occurs because the modulation alphabet grows in size with higher modulation levels, necessitating the inclusion of more terms in the polynomial expression.

4.3.1 LLR Calculation and Generating LUTs

The log-likelihood ratio (LLR) of the ith bit ($\mathbf{a_i}$) is calculated as follows:

$$\lambda_i = \log \frac{\sum_{L_i,+1} f(\mathbf{y}|\mathbf{a},\mathbf{V}) P(\mathbf{a})}{\sum_{L_i,-1} f(\mathbf{y}|\mathbf{a},\mathbf{V}) P(\mathbf{a})}, \tag{4.22}$$

where $P(\mathbf{a})$ is the probability of occurrence of sequences with ith bit being +1 or -1. $L_i,+1$ and $L_i,-1$ are the sets of sequences with ith bit being +1 and -1, respectively, $i = 1, 2, ..., N-1, N$. $f(\mathbf{y}|\mathbf{a},\mathbf{V})$ is the likelihood of the received signal $\mathbf{y}$ given $\mathbf{a}$ and $\mathbf{V}$,

and is calculated from

$$f(\mathbf{y}|\mathbf{a},\mathbf{V}) = \frac{1}{\sqrt{|\Sigma|(2\pi)^N}} e^{-\frac{1}{2}(\mathbf{y}-\mathbf{V}\hat{\mathbf{a}}-\boldsymbol{\mu})\Sigma^{-1}(\mathbf{y}-\mathbf{V}\hat{\mathbf{a}}-\boldsymbol{\mu})^{\mathbf{T}}}, \tag{4.23}$$

where $\boldsymbol{\mu}$ and $\boldsymbol{\Sigma}$ correspond to zero mean and the covariance of $\sigma^2\mathbf{I}$, respectively, within the multivariate Gaussian noise pdf. The determinant of the covariance matrix is denoted by $|\boldsymbol{\Sigma}|$. Instead of searching for the vector space online, lookup tables are generated offline to get the LLR directly. We sort the stages of generation of the LUTs for M-PAM as follows:

- Determine $\frac{E_s}{N_o}$ in an uncoded SDR detector based on the modulation level, the intended code rate, and $\frac{E_{mb}}{N_o}$, where E_{mb} represents the energy of the message bit.
- Transmit R symbol sequences of length N.
- Pass them through the channel.
- Get the outputs x_n of the uncoded SDR based FTN detector.
- Obtain the histogram of the x_n by dividing the range of $[\min(1-2^{m+1})\ \ \max(2^{m+1}-1)]$, $m = 0, 1, ..., \log_2 M - 2, \log_2 M - 1$, in which interval the detector outputs, to J bins. Based on the positions of transmit bits, c_n^m of the symbol a_n, obtain the histograms of conditional probability density functions $f(x_n|c_n^m = 1)$, $f(x_n|c_n^m = 0)$ in Equation **4.23** using the output of the detector x_n. Please note that while obtaining the conditional pdfs we do not use the the matched filter output y but the detector output x_n, maximum likelihood decoding of which gives $\hat{a}$.
- Get the look-up tables by calculating the LLRs,λ_n^m as in Equation **4.24** for every bit of the symbol for the $\frac{E_s}{N_o}$ dB of interest.

$$\begin{aligned}\lambda_n^m &= \log\frac{Pr(c_n^m = 0|x_n)}{Pr(c_n^m = 1|x_n)},\\ &= \log\frac{f(x_n|c_n^m = 0)Pr(c_n^m = 0)/f(x_n)}{f(x_n|c_n^m = 1)Pr(c_n^m = 1)/f(x_n)},\\ &= \log\frac{f(x_n|c_n^m = 0)}{f(x_n|c_n^m = 1)}.\end{aligned} \tag{4.24}$$

- Apply the curvefitting operation to the tables to remove the discontinuities in them that causes the channel decoder not to work well. In the curvefitting stage, we break the unfitted curve in Figure 4.7 and Figure 4.8 into three parts. In the first and third parts of the curves corresponding to the ranges of $(-3,-1)$ and $(1,3)$, respectively, we fit them using the first-degree polynomial. When it comes to the range of $(-1,1)$ the second- and third-degree polynomials are fitted with the mentioned part for λ_n^0 and λ_n^1, respectively.

- Find the LLR index corresponding to the detector output using

$$x_{index}^n = \min(\max(\text{floor}((x_n + \max(2^{m+1}-1))J/M) + 1, 1), J), \tag{4.25}$$

  where x_n is the output of the detector.

- Pick the corresponding LLR from LUT.

4.4 Complexity Analysis

The complexity of the semidefinite relaxation based optimization method is $O(N^{3.5})$ as expressed in [45]. In the complexity comparison, we do not take the offline generation of the LUTs into account, thus, the soSDR can be said to have a complexity of $O(N^{3.5})$, similar to the hard-output SDR detector. While the soSDR and BCJR detectors have polynomial time complexity for higher modulation levels the former has a significant advantage over the BCJR detector because its complexity does not depend on the ISI length with which the BCJR detector has an exponentially increasing complexity [38].

4.5 Simulation Results

In this section, we evaluate the performance of the proposed soSDR detector for a coded FTN signaling system over an additive white Gaussian noise (AWGN) channel. The proposed soSDR is simulated for the value of $\tau = 0.8$. In the simulations, we work on the 4-PAM with Gray coding and a root raised cosine filter with roll-off factor $\alpha = 0.5$ are adopted. In the generation of the look-up tables, we set the number of transmit sequences R to 10000, the number of bins J to 300. For channel coding, polar codes of rate of $3/4$ and codeword length of $N = 256$ are used.

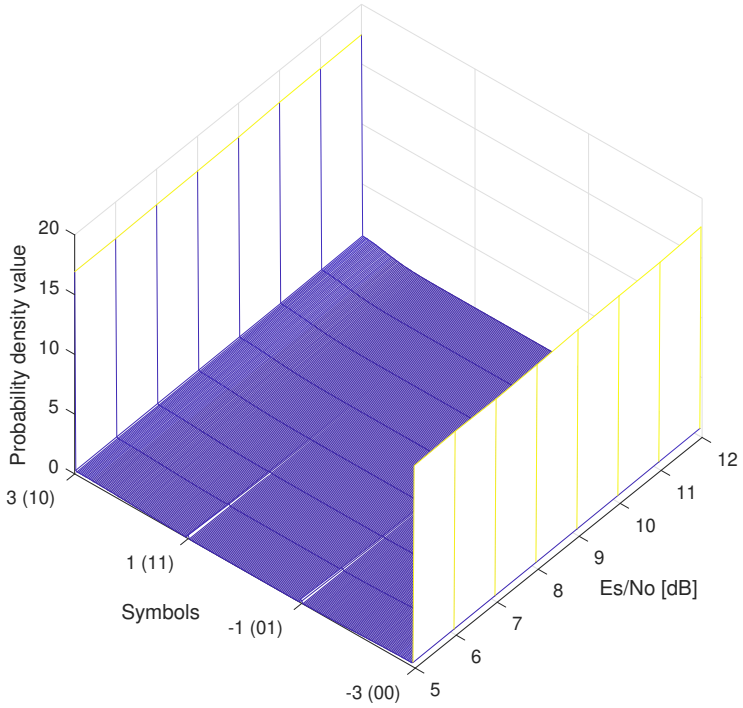

Figure 4.3 Histogram of the conditional pdf $f(x_n|c_n^0 = 0)$.

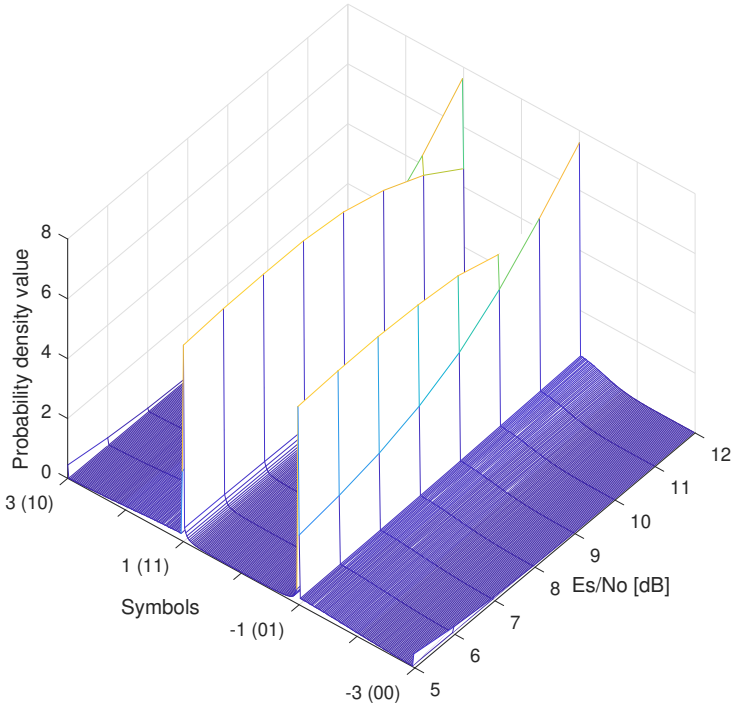

Figure 4.4 Histogram of the conditional pdf $f(x_n|c_n^0 = 1)$.

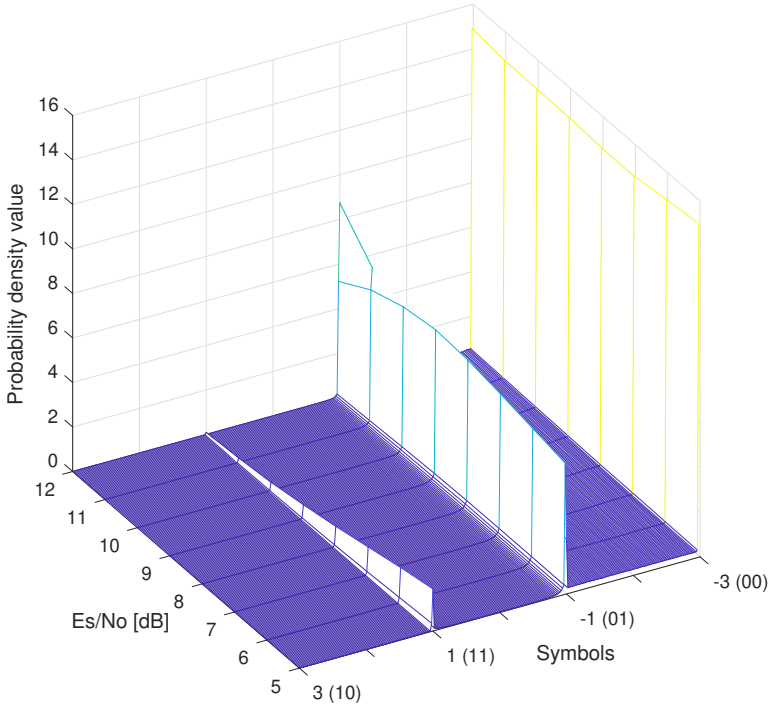

Figure 4.5 Histogram of the conditional pdf $f(x_n|c_n^1 = 0)$.

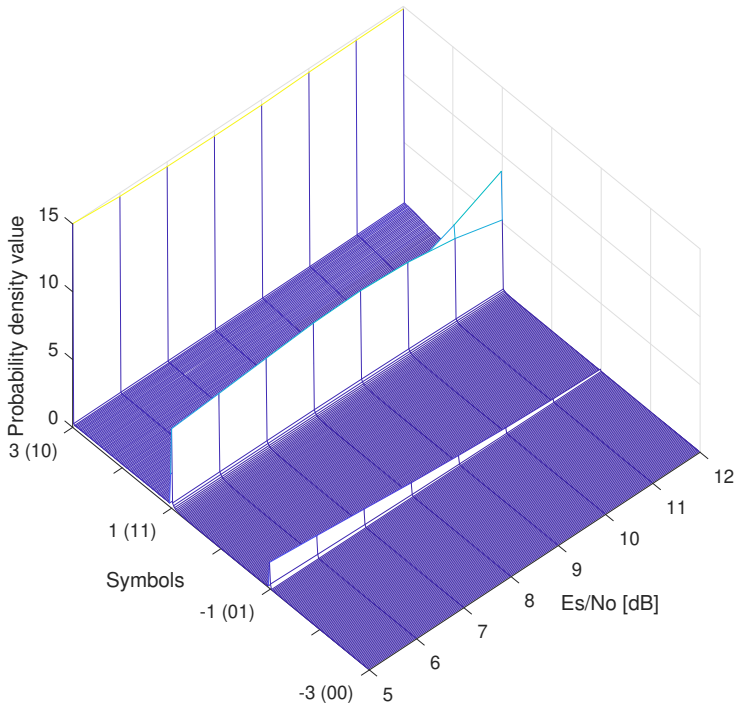

Figure 4.6 Histogram of the conditional pdf $f(x_n|c_n^1 = 1)$.

Figures 4.3, 4.4, 4.5, and 4.6 depict the histograms of conditional probability density functions $f(x_n|c_n^0 = 0)$, $f(x_n|c_n^0 = 1)$, $f(x_n|c_n^1 = 0)$, and $f(x_n|c_n^1 = 1)$ for the SDR detector, respectively.

When the least significant bit (LSB) of the transmitted symbol is set to 0, the probability of the symbols being either -3 or 3 becomes nearly equal, as evident in the data presented in Figure 4.3. In Figure 4.4, The detector appears to exhibit erroneous decisions when operating at low $\frac{E_s}{N_0}$ values, such as 5 dB and 6 dB. As the $\frac{E_s}{N_0}$ ratio increases, the probability of making decisions of both -1 and $+1$ becomes more pronounced since LSB = 1.

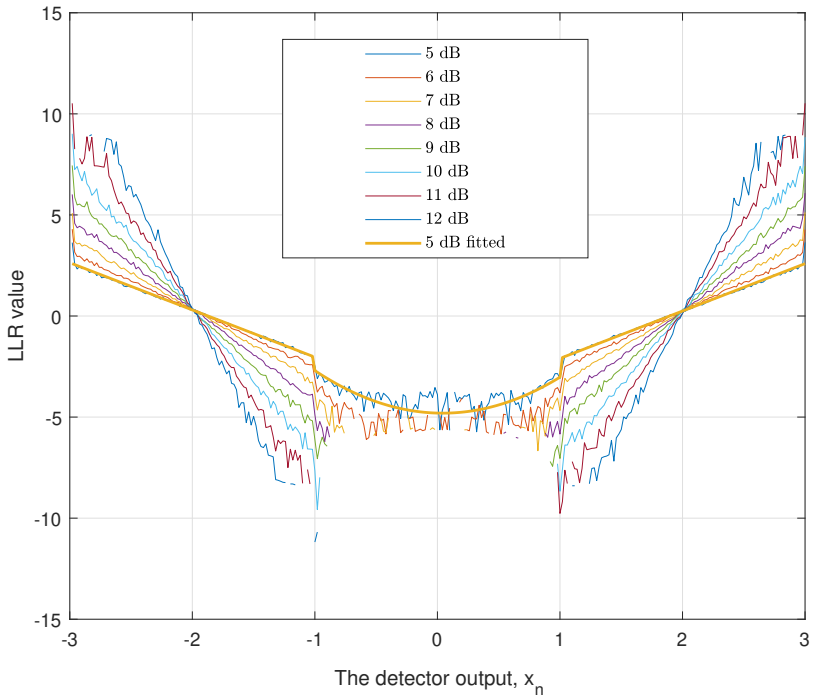

Figure 4.7 LLR values generated for the least significant bit λ_n^0.

Regarding the histograms of conditional probability density functions when the most significant bit is known, Figure 4.5 and Figure 4.6 indicate that the detector tends to choose symbols 3 and 1 more frequently than symbols -1 and -3, respectively. Additionally, in Figures 4.7 and 4.8, we have plotted the log-likelihood ratios (LLRs) for both the least significant bit (LSB) and the most significant bit (MSB) at different $\frac{E_s}{N_0}$ values. It is evident that there are discontinuities present in the LLRs, which necessitates the use of curve-fitting operations. Depending on the output value from

the detector, we extract the fitted value from the LSB and MSB tables.

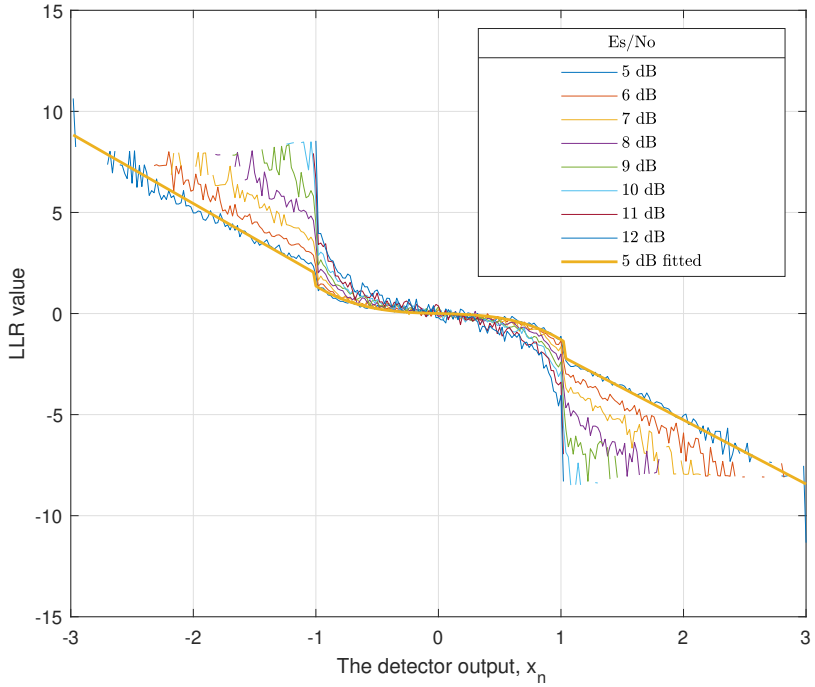

Figure 4.8 LLR values generated for most significant bit λ_n^1.

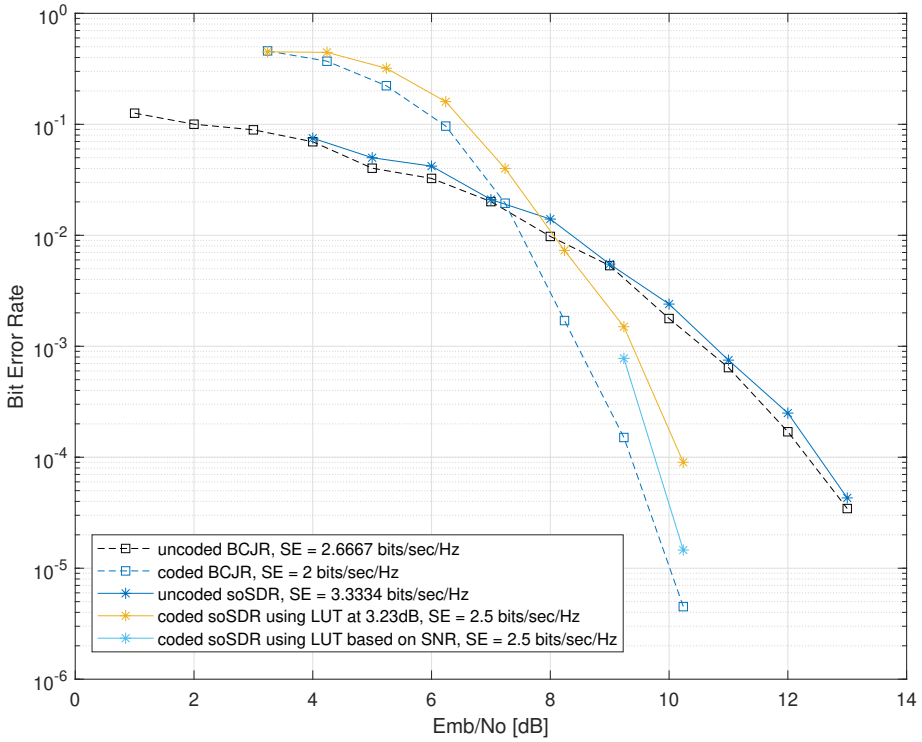

Figure 4.9 BER performance of soSDR.

Finally, we demonstrate the BER performance of the uncoded and polar coded FTN system with the soSDR detector. At the BER of 10^{-4}, the detector almost follows the BCJR performance, there is a gap of 0.1 dB between them at the BER of 10^{-4}. It also achieves spectral efficiency (SE) of 1.6667 bits/sec/Hz in the uncoded scenario, compared to the SE of 1.3334 bits/sec/Hz in the Nyquist signaling, meaning that the FTN signaling can provide $\frac{1.6667-1.3334}{1.6667} = 25\%$ more SE than the Nyquist signaling. In the coded case, with the code rate (CR) of $\frac{3}{4}$, the SE reduces to 1.25 bits/sec/Hz and at the same BER of 10^{-4}, the performance of the detector is 0.8 dB away from the BCJR, using the LUT at $\frac{E_s}{N_o}$ = 5 dB; i.e, at $\frac{E_{mb}}{N_o}$ = 3.23 dB since $\frac{E_{mb}}{N_o} = \frac{E_s}{N_o}$ - $10\log_{10}(m)$ - $10\log_{10}(\text{CR})$. Moreover, if the lookup table based on each SNR per symbol is used the detector can approach 0.3 dB more to the BCJR, showing how good the SNR based lookup tables have effect on the performance.

CHAPTER 5

CONCLUSION AND DISCUSSION

In this thesis, we examine the complexity of FTN signaling within both coded and uncoded scenarios, focusing on key parameters such as the value of τ and the roll-off factor α. By employing polar codes, the performance loss introduced by the SSSgbKSE detection system is mitigated by 1.2 dB, 3.1 dB, and 1 dB when $\tau = 0.8$, $\tau = 0.7$, and $\tau = 0.6$, respectively. The most significant performance gain achieved through polar codes is 3.1 dB at $\tau = 0.7$. However, at $\tau = 0.6$, the coding gain diminishes due to the inability of the SSSgbKSE algorithm to generate accurate LLR values under high Inter-Symbol Interference (ISI) conditions. As a consequence of this study, polar codes mitigate the performance degradation resulting from the detector's low complexity, while preserving the reduced complexity. When it comes to the FTN signaling implemented with NB-LDPC codes, it is evident that for high values of τ, the utilization of high complexity FTN signaling detectors with LDPC codes does not yield significant benefits. Instead, with NB-LDPC codes, a low-complexity FTN signaling detector proves sufficient in achieving the desired performance.

The thesis also introduces a novel component interleaving method known as CI-FTN, which induces constructive Inter-Symbol Interference (ISI) among the counter-clockwise rotated BPSK symbols. Additionally, a low-complexity FTN detector is introduced. The performance and complexity of this proposed detector are juxtaposed against standard FTN systems. Simulation results vividly illustrate that when $\tau = 0.5$, the CI-FTN detector achieves an equivalent performance to QPSK Nyquist signaling (where ISI is absent, $\tau = 1$). At $\tau = 0.45$, the proposed CI-FTN method attains a 10% increase in spectral efficiency (SE) compared to QPSK Nyquist signaling, albeit at an energy per bit expense of 0.6 dB. As a result, the CI-FTN signaling offers an intriguing compromise between performance and complexity.

Finally, the investigation of low-complexity soft-output detection algorithms becomes imperative in the context of channel coding and high modulation levels. It is equally crucial to design a detector capable of generating reliable soft outputs, particularly

tailored for high modulation scenarios. To address this, the thesis introduces a novel soft-output Semidefinite Relaxation (soSDR) based FTN detector, which exhibits adaptability to high modulation levels. Remarkably, the proposed detector introduces minimal additional complexity through the utilization of lookup tables (LUTs) derived from detector outputs. Given that modulation constellations can be represented through polynomial equations, and the initially nonconvex FTN signaling detection challenge transforms into a convex optimization problem following semidefinite relaxation, the chosen modulation type and level for this study is M-PAM ($M = 4$).

The performance of the detector is evaluated by comparing it with the optimal BCJR detector. In the uncoded scenario, the detector exhibits an impressive performance, achieving a proximity of 0.1 dB to the BCJR at a bit error rate (BER) of 10^{-4}. Moving into the coded scenario, a gap of 0.8 dB remains between the soSDR detector and BCJR, both operating at the same bit error rate. However, this gap narrows to 0.5 dB when the signal-to-noise ratio based look-up table (LUT) is integrated. Considering the low-complexity, the results show that the soSDR that is adaptable to high modulation provides good performance with the log-likelihoods produced.

As a discussion section, some of our thoughts on challenges, open research topics, and future research directions are shared below:

1. The performance of the low-complexity detector can be assessed across various turbo code schemes, and new low-complexity approaches can be devised based on the specific characteristics of the channel coding used.

2. In the context of the CI-FTN signaling, its applicability can be extended to higher modulation levels as well as multiple input multiple output (MIMO) systems.

3. Incorporating detection into the iterative structure of channel coding can enhance performance.

4. Unlike conventional methods, novel approaches better suited for the FTN signaling can be explored for tasks such as channel estimation, synchronization, and multicarrier communications.

5. One of the ongoing research challenges is achieving satisfactory performance with a reasonable level of complexity when compared to the optimal detector, particularly at lower values of τ for higher modulation levels.

6. Reducing τ to significantly lower values may encounter a constraint imposed by super-oscillation. This situation requires analysis from an information theory standpoint.

7. Examining FTN signaling studies within the thesis across various channel environments can be considered as prospective areas for future research.

8. Implementing all communication systems using FTN signaling in experimental setups like FPGAs would be an appealing approach. This would allow us to showcase the hardware complexity introduced by the detector or FTN signaling in a real system, enabling a comparison with the conventional approach.

REFERENCES

[1] Lender A., "The duobinary technique for high-speed data transmission," *IEEE Transactions on Communication and Electronics*, vol. 82, no. 2, pp. 214–218, 1963.

[2] Smith J. W., "The joint optimization of transmitted signal and receiving filter for data transmission systems," *The Bell System Technical Journal*, vol. 44, no. 10, pp. 2363–2392, 1965.

[3] Berger T. and Tufts D., "Optimum pulse amplitude modulation: Transmitter-receiver design and bounds from information theory," *IEEE Transactions on Information Theory*, vol. 13, no. 2, pp. 196–208, 1967.

[4] Tufts D., "Nyquist's problem—the joint optimization of transmitter and receiver in pulse amplitude modulation," *Proceedings of the IEEE*, vol. 53, no. 3, pp. 248–259, 1965.

[5] Forney G., "Maximum-likelihood sequence estimation of digital sequences in the presence of intersymbol interference," *IEEE Transactions on Information Theory*, vol. 18, no. 3, pp. 363–378, 1972.

[6] Omura J., "Optimal receiver design for convolutional codes and channels with memory via control theoretical concepts," *Inform. Sci.*, pp. 243–266, 1971.

[7] Mazo J. E., "Faster-than-nyquist signaling," *The Bell System Technical Journal*, vol. 54, no. 8, pp. 1451–1462, 1975.

[8] Liveris A. D. and Georghiades C. N., "Exploiting faster-than-Nyquist signaling," *IEEE J COM*, vol. 51, no. 9, pp. 1502–1511, Sep. 2003.

[9] Anderson J. B., Prlja A., and Rusek F., "New reduced state space BCJR algorithms for the ISI channel," in *Proc. IEEE Int. Symp. Inf. Theory (ISIT)*, Seoul, Korea, Jun. 2009, pp. 889–893.

[10] Prlja A., Anderson J. B., and Rusek F., "Receivers for faster-than-Nyquist signaling with and without turbo equalization," in *Proc. IEEE Int. Symp. Inf. Theory (ISIT)*, Toronto, Canada, Jul. 2008, pp. 464–468.

[11] Prlja A. and Anderson J. B., "Reduced-complexity receivers for strongly narrowband intersymbol interference introduced by faster-than-Nyquist signaling," *IEEE_J_COM*, vol. 60, no. 9, pp. 2591–2601, Sep. 2012.

[12] Bedeer E., Yanikomeroglu H., and Ahmed M. H., "Low complexity detection of M-ary PSK faster-than-nyquist signaling," in *Proc. IEEE Wireless Communications and Networking Conference (WCNC) - Workshop on Ultra-High Speed, Low Latency and Massive Connectivity Communication (UHSLLC) for 5G/B5G*, Marrakech, Morocco, May 2019, pp. 1–6.

[13] Yu T., Zhao M., Zhong J., and Cai Y., "Low-Complexity Detection for FTN Signaling Based on Weighted FG-SS-BP Equalization Method," in *Proc. IEEE Vehicular Technology Conference (VTC Spring)*, Sep. 2016, pp. 1–5.

[14] Fukumoto H. and Hayashi K., "Overlap frequency domain equalization for faster-than-Nyquist signaling," *arXiv preprint arXiv:1509.00562*, 2015.

[15] Bedeer E., Ahmed M. H., and Yanikomeroglu H., "Low-complexity detection of high-order QAM faster-than-Nyquist signaling," *IEEE Access*, vol. 5, pp. 14 579–14 588, 2017.

[16] Kulhandjian M., Bedeer E., Kulhandjian H., D'Amours C., and Yanikomeroglu H., "Low-complexity detection for faster-than-Nyquist signaling based on probabilistic data association," *IEEE Communications Letters*, vol. 24, no. 4, pp. 762–766, 2020.

[17] Bedeer E., Ahmed M. H., and Yanikomeroglu H., "A very low complexity successive symbol-by-symbol sequence estimator for faster-than-Nyquist signaling," *IEEE Access*, vol. 5, pp. 7414–7422, 2017.

[18] Tajan R., Benammar B., Poulliat C., and Boucheret M., "On coding for faster-than-nyquist signaling," in *2015 IEEE International Black Sea Conference on Communications and Networking (BlackSeaCom)*, May 2015, pp. 92–96.

[19] Ovsyannikova A. S., Zavjalov S. V., and Volvenko S. V., "On the joint use of optimal faster than nyquist signals with polar and turbo codes," in *2018 IEEE International Conference on Electrical Engineering and Photonics (EExPolytech)*, Oct 2018, pp. 79–82.

[20] Anderson J. B. and Prlja A., "Turbo equalization and an M-BCJR algorithm for strongly narrowband intersymbol interference," in *Proc. IEEE International Symposium On Information Theory & Its Applications*, Oct. 2010, pp. 261–266.

[21] Maalouli G. and Bannister B. A., "Performance analysis of a mmse turbo equalizer with ldpc in a ftn channel with application to digital video broadcast," in *2014 48th Asilomar Conference on Signals, Systems and Computers*, Nov 2014, pp. 1871–1875.

[22] Caglan A., Cicek A., Cavus E., Bedeer E., and Yanikomeroglu H., "Polar coded faster-than-Nyquist (FTN) signaling with symbol-by-symbol detection," in *2020 IEEE Wireless Communications and Networking Conference (WCNC), virtual conference*, 2020, pp. 1–5.

[23] Cerci E., Çiçek A., Cavus E., Bedeer E., and Yanikomeroglu H., "Coded faster-than-nyquist signaling for short packet communications," in *Proc. 32nd IEEE Annual International Symposium on Personal, Indoor and Mobile Radio Communications, PIMRC 2021, Helsinki, Finland, Sep., 2021*. IEEE, 2021, pp. 428–433. [Online]. Available: https://doi.org/10.1109/PIMRC50174.2021.9569719

[24] Arikan E., "Channel polarization: A method for constructing capacity-achieving codes for symmetric binary-input memoryless channels," *IEEE Transactions on Information Theory*, vol. 55, no. 7, pp. 3051–3073, 2009.

[25] Song S., Lin J., Tian J., and Wang Z., "A reduced complexity decoding algorithm for nb-ldpc codes," in *2017 IEEE 17th International Conference on Communication Technology (ICCT)*, 2017, pp. 127–131.

[26] El Hassani S., Hamon M.-H., and Pénard P., "A comparison study of binary and non-binary ldpc codes decoding," in *SoftCOM 2010, 18th International*

Conference on Software, Telecommunications and Computer Networks, 2010, pp. 355–359.

[27] Voicila A., Declercq D., Verdier F., Fossorier M., and Urard P., "Low-complexity, low-memory ems algorithm for non-binary ldpc codes," in *2007 IEEE International Conference on Communications*, 2007, pp. 671–676.

[28] Cicek A., Cavus E., Bedeer E., Marsland I., and Yanikomeroglu H., "Coordinate interleaved faster-than-nyquist signaling," *IEEE Communications Letters*, vol. 27, no. 1, pp. 229–233, 2023.

[29] Sugiura S., "Frequency-domain equalization of faster-than-Nyquist signaling," *IEEE Wireless Communications Letters*, vol. 2, no. 5, pp. 555–558, Oct. 2013.

[30] Li S., Bai B., Zhou J., Chen P., and Yu Z., "Reduced-complexity equalization for faster-than-Nyquist signaling: New methods based on Ungerboeck observation model," *IEEE Transactions on Communications*, vol. 66, no. 3, pp. 1190–1204, Nov. 2018.

[31] Liu B., Li S., Xie Y., and Yuan J., "A novel sum-product detection algorithm for faster-than-Nyquist signaling: A deep learning approach," *IEEE Transactions on Communications*, vol. 69, no. 9, pp. 5975–5987, Jun. 2021.

[32] Wang H., Liu A., Feng Z., Liang X., Liang H., and Cai B., "Iterative-detection-aided Tomlinson-Harashima precoding for faster-than-Nyquist signaling," *IEEE Access*, vol. 8, pp. 7748–7757, 2020.

[33] Li Q., Gong F.-K., Song P.-Y., Li G., and Zhai S.-H., "Beyond DVB-S2X: Faster-than-Nyquist signaling with linear precoding," *IEEE Transactions on Broadcasting*, vol. 66, no. 3, pp. 620–629, Sep. 2020.

[34] Li Y., Xiao S., Wang J., and Tang W., "Cholesky-decomposition aided linear precoding and decoding for FTN signaling," *IEEE Wireless Communications Letters*, vol. 10, no. 6, pp. 1163–1167, Jun. 2021.

[35] Boutros J. and Viterbo E., "Signal space diversity: A power- and bandwidth-efficient diversity technique for the Rayleigh fading channel," *IEEE Transactions on Information Theory*, vol. 44, no. 4, pp. 1453–1467, Jul. 1998.

[36] Wang H., Liu A., Liang X., Peng S., and Wang K., "Linear precoding for faster-than-Nyquist signaling," in *Proc. IEEE International Conference on Computer and Communications*, 2017, pp. 52–56.

[37] Cicek A., Cavus E., Bedeer E., Marsland I., and Yanikomeroglu H., "Low-complexity lookup table aided soft-output semidefinite relaxation based ftn signaling detector," *submitted to the IEEE Communications Letters*, 2023.

[38] Anderson J. B., Rusek F., and Öwall V., "Faster-than-Nyquist signaling," *IEEE_J_PROC*, vol. 101, no. 8, pp. 1817–1830, Aug. 2013.

[39] Modenini A., Rusek F., and Colavolpe G., "Faster-than-Nyquist signaling for next generation communication architectures," in *Proc. European Signal Processing Conference (EUSIPCO)*, Lisbon, Portugal, Sep. 2014, pp. 1856–1860.

[40] Bedeer E., Yanikomeroglu H., and Ahmed M. H., "Reduced complexity optimal detection of binary faster-than-Nyquist signaling," in *Proc. IEEE International Conference on Communications (ICC)*, Paris, France, May 2017, pp. 1–6.

[41] Wang Q., Xie Q., Wang Z., Chen S., and Hanzo L., "A universal low-complexity symbol-to-bit soft demapper," *IEEE Transactions on Vehicular Technology*, vol. 63, no. 1, pp. 119–130, 2014.

[42] Kang I.-W., Shin J.-W., and Kim H.-N., "Low-complexity llr calculation for gray-coded pam modulation," *IEEE Communications Letters*, vol. 20, no. 4, pp. 688–691, 2016.

[43] Leroux C., Tal I., Vardy A., and Gross W. J., "Hardware architectures for successive cancellation decoding of polar codes," in *Proc. IEEE International Conference on Acoustics, Speech and Signal Processing (ICASSP)*, Prague, Czech Republic, May 2011, pp. 1665–1668.

[44] Ma W.-K., *Semidefinite Relaxation and Its Application in Signal Processing and Communications*. Xi'an, China: MIIS Tutorial, Jul. 2012.

[45] Luo Z.-Q., Ma W.-K., So A. M.-C., Ye Y., and Zhang S., "Semidefinite relaxation of quadratic optimization problems," *IEEE M SP*, vol. 27, no. 3, p. 20, May 2010.

APPENDICES

Appendix A: Proof of the Nyquist condition for zero ISI in the frequency domain.

Appendix B: Proof that the FTN signaling uses the same energy as the Nyquist signaling.

Appendix C: Noise covariance after the matched filter in FTN signaling

Appendix A – Proof of the Nyquist condition for zero ISI.

Let $x(t)$ be the inverse Fourier transform of $X(f)$.

$$x(t) = \int_{-\infty}^{\infty} X(f)e^{j2\pi ft}df \tag{A.1}$$

After sampling Equation A.1 at $t = kT$, it turns to Equation A.2,

$$x(kT) = \int_{-\infty}^{\infty} X(f)e^{j2\pi fkT}df \tag{A.2}$$

which can also be written as

$$\begin{aligned} x(kT) &= \Sigma_{-\infty}^{\infty} \int_{\frac{(2m-1)}{2T}}^{\frac{(2m+1)}{2T}} X(f)e^{j2\pi fkT}df \\ &= \Sigma_{-\infty}^{\infty} \int_{\frac{-1}{2T}}^{\frac{1}{2T}} X(f+\frac{m}{T})e^{j2\pi fkT}df \\ &= \int_{\frac{-1}{2T}}^{\frac{1}{2T}} [\Sigma_{-\infty}^{\infty} X(f+\frac{m}{T})]e^{j2\pi fkT}df \\ &= \int_{\frac{-1}{2T}}^{\frac{1}{2T}} Z(f)e^{j2\pi fkT}df, \end{aligned} \tag{A.3}$$

where $Z(f) = \Sigma_{-\infty}^{\infty} X(f+\frac{m}{T})$. Since $Z(f)$ is a periodic function with $\frac{1}{T}$ it can be expressed in terms of Fourier series as

$$Z(f) = \Sigma_{k-\infty}^{\infty} z_k e^{j2\pi fkT}, \tag{A.4}$$

where

$$z_k = T\int_{-\frac{1}{2T}}^{\frac{1}{2T}} Z(f)e^{-j2\pi fkT}df. \tag{A.5}$$

From the relation between the Equation A.3 and Equation A.5

$$z_k = T\,x(-kT). \tag{A.6}$$

Hence, the necessary condition satisfying Equation A.7

$$x(kT) = \begin{cases} 1, & k = 0 \\ 0, & k \neq 1 \end{cases} \tag{A.7}$$

is as follows:

$$z_k = \begin{cases} T, & k = 0 \\ 0, & k \neq 1 \end{cases} \tag{A.8}$$

which means $Z(f) = T$ or, in other words, $\Sigma_{m=\infty}^{-\infty} X(f + \frac{m}{T}) = T$

Appendix B – Proof that FTN signaling uses the same energy.

The output of the transmit filter in the faster-than-Nyquist signaling is defined as

$$s(t) = \text{sqrt}(E_s)\Sigma_{n=0}^{N-1} a_n h(t - n\tau T) \tag{B.1}$$

The average energy s(t) can be defined as

$$\begin{aligned}
E_{av,s(t)} &= \mathbb{E}\left\{\int_{-\infty}^{\infty} |s(t)|^2 dt\right\} \\
&= \mathbb{E}\left\{E_s \int_{-\infty}^{\infty} \Sigma_{n=0}^{N-1} a_n h(t - n\tau T)\Sigma_{m=0}^{M-1} a_m^* h^*(t - m\tau T)dt\right\} \\
&= \mathbb{E}\left\{E_s \int_{-\infty}^{\infty} \Sigma_{n=0}^{N-1}\Sigma_{m=0}^{M-1} a_n a_m^* h(t - n\tau T)h^*(t - m\tau T)dt\right\} \\
&= \mathbb{E}\left\{E_s \Sigma_{n=0}^{N-1}\Sigma_{m=0}^{M-1} a_n a_m^* g((n-m)\tau T)\right\} \\
&= E_s \Sigma_{n=0}^{N-1}\Sigma_{m=0}^{M-1} \mathbb{E}\{a_n a_m^*\} g((n-m)\tau T) \\
&= E_s \Sigma_{n=0}^{N-1} \mathbb{E}\{a_n a_n^*\} g(0) \\
&= E_s \Sigma_{n=0}^{N-1} 1 \\
&= E_s N
\end{aligned} \tag{B.2}$$

Hence the average energy per symbol $E_{av,symbol} = \frac{E_s N}{N} = E_s$.

Appendix C – Noise covariance after the matched filter in FTN signaling.

Covariance of the noise after the matched filter in the FTN signaling is as follows:

$$\begin{aligned}\mathrm{Cov}(q(t_1),q(t_2)) &= \mathbb{E}\Big[\,[q(t_1)-\mathbb{E}(q(t_1))]\,[q(t_2)-\mathbb{E}(q(t_2))]\,\Big] \\ &= \mathbb{E}\left[\int_{-\infty}^{\infty} w(t_1)h(t_1-n\tau T)dt_1 \int_{-\infty}^{\infty} w(t_2)h(t_2-m\tau T)dt_2\right] \\ &= \int_{-\infty}^{\infty}\int_{-\infty}^{\infty} \mathbb{E}[w(t_1)w(t_2)]\,h(t_1-n\tau T)h(t_2-m\tau T)dt_1dt_2\end{aligned} \tag{C.1}$$

Since $\mathbb{E}[w(t_1)w(t_2)] = \sigma^2\delta(t_1-t_2)$ Equation C.1 turns to

$$\begin{aligned}\mathrm{Cov}(q(t_1),q(t_2)) &= \sigma^2 \int_{-\infty}^{\infty} h(t_1-n\tau T)h(t_1-m\tau T)dt_1 \\ &= \sigma^2 G_{n,m}\end{aligned} \tag{C.2}$$

where G is non-diagonal matrix, meaning that noise samples are not independent anymore.